

Identification and analysis of splicing quantitative trait loci across multiple tissues in the human genome

Diego Garrido-Martín¹, Beatrice Borsari¹, Miquel Calvo², Ferran Reverter² and Roderic Guigó^{*1,3}

¹Centre for Genomic Regulation (CRG), The Barcelona Institute of Science and Technology, Dr. Aiguader 88, Barcelona 08003, Catalonia, Spain

²Section of Statistics, Faculty of Biology, Universitat de Barcelona (UB), Av. Diagonal 643, Barcelona 08028, Spain

³Universitat Pompeu Fabra (UPF), Barcelona, Catalonia, Spain

*Correspondence should be addressed to E-mail: roderic.guigo@crg.eu (Roderic Guigó)

Abstract

We have developed an efficient and reproducible pipeline for the discovery of genetic variants affecting splicing (sQTLs), based on an approach that captures the intrinsically multivariate nature of this phenomenon. We employed it to analyze the multi-tissue transcriptome GTEx dataset, generating a comprehensive catalogue of sQTLs in the human genome. A core set of these sQTLs is shared across multiple tissues. Downstream analyses of this catalogue contribute to the understanding of the mechanisms underlying splicing regulation. We found that sQTLs often target the global splicing pattern of genes, rather than individual splicing events. Many of them also affect gene expression, but not always of the same gene, potentially uncovering regulatory loci that act on different genes through different mechanisms. sQTLs tend to be preferentially located in introns that are post-transcriptionally spliced, which would act as hotspots for splicing regulation. While many variants affect splicing patterns by directly altering the sequence of splice sites, many more modify the binding of RNA-binding proteins (RBPs) to target sequences within the transcripts. Genetic variants affecting splicing can have a phenotypic impact comparable or even stronger than variants affecting expression, with those that alter RBP binding playing a prominent role in disease.

1 Introduction

2 Alternative splicing (AS) is the process through which multiple transcript isoforms are produced from a
3 single gene¹. It is a key mechanism that increases functional complexity in higher eukaryotes². Often, its
4 alteration leads to pathological conditions³. AS is subject to a tight regulation, usually tissue-, cell type- or
5 condition-specific, that involves a wide range of *cis* and *trans* regulatory elements^{4,5}. Since AS is generally
6 coupled with transcription, transcription factors and chromatin structure also play a role in its regulation⁶.

7 In recent years, transcriptome profiling of large cohorts of genotyped individuals by RNA-seq has al-
8 lowed the identification of genetic variants affecting AS, i.e. splicing quantitative trait loci or sQTLs⁷⁻¹².
9 sQTL analyses in a variety of experimental settings have helped to gain insight into the mechanisms un-
10 derlying GWAS associations for a number of traits, such as adipose-related traits¹³, Alzheimer's disease¹⁰,
11 schizophrenia⁹ or breast cancer¹⁴, among others. sQTLs might actually contribute to complex traits and
12 diseases at a similar or even larger degree than variants affecting gene expression¹⁵.

13 The vast majority of methods commonly used for sQTL mapping treat splicing as a univariate pheno-
14 type. They assess association between genetic variants and the abundance of individual transcripts^{7,16}, or
15 the splicing of individual exons^{9,17} or introns^{12,15}. However, this approach ignores the strongly correlated
16 structure of AS measurements (e.g. at constant gene expression level, higher levels of a splicing isoform
17 correspond necessarily to lower levels of other isoforms). In contrast, we propose an approach that takes
18 into account the intrinsically multivariate nature of alternative splicing: variants are tested for association
19 with a vector of AS phenotypes, such as the relative abundances of the transcript isoforms of a gene or the
20 intron excision ratios of an intron cluster obtained by LeafCutter¹⁸.

21 Based on this approach, we have developed a pipeline for efficient and reproducible sQTL mapping.
22 We have employed it to leverage the multi-tissue transcriptome data generated by the Genotype-Tissue Ex-
23 pression (GTEx) Consortium, producing a comprehensive catalogue of genetic variants affecting splicing
24 in the human genome. Downstream analyses of this catalogue uncover a number of relevant features re-
25 garding splicing regulation. Thus, consistent with the multivariate nature of splicing, we have observed that
26 sQTLs tend to involve multiple splicing events. A substantial fraction of sQTLs also affects gene expression,
27 a reflection of the intimate relationship between splicing and transcription. We have found, however, many
28 cases in which the sQTL affects the expression of a gene other than the sQTL target. In these cases, the
29 pleiotropic effect of the regulatory locus is not mediated by the interplay between the splicing and transcrip-
30 tion processes, but it is exerted through different mechanisms, acting upon different genes that otherwise
31 may not appear to be directly interacting. We have also found that sQTLs tend to be preferentially located
32 in introns that are post-transcriptionally spliced: these introns would be consequently acting as hotspots
33 for splicing regulation. While many variants affect splicing patterns by directly altering the sequence of
34 splice sites, many more modify the binding of RNA-binding proteins (RBPs) to target sequences within
35 the transcripts. We have observed that sQTLs often impact GWAS traits and diseases more than variants
36 affecting only gene expression, confirming earlier reports which suggest that splicing mutations underlie
37 many hereditary diseases^{15,19}. For many conditions, GWAS associations are particularly strong for sQTLs

38 altering RBP binding sites.

39 Results

40 Identification of *cis* splicing QTLs across GTEx tissues

41 For sQTL mapping, we developed `sQTLseeker2`, a software based on `sQTLseeker`²⁰, which identifies
42 genetic variants associated with changes in the relative abundances of the transcript isoforms of a
43 given gene. `sQTLseeker` uses the Hellinger distance to estimate the variability of isoform abundances
44 across observations, and Anderson's method^{21,22}, a non-parametric analogue to multivariate analysis
45 of variance, to assess the significance of the associations (see Methods and Supplementary Note 1).
46 Among other enhancements, `sQTLseeker2` improves the accuracy and speed of the *p* value calculation,
47 and allows to account for additional covariates before testing for association with the genotype,
48 while maintaining the multivariate statistical test in `sQTLseeker`. It also implements a multiple testing
49 correction scheme that empirically characterizes, for each gene, the distribution of *p* values expected under
50 the null hypothesis of no association (see Methods and Supplementary Note 1). To ensure highly
51 parallel, portable and reproducible sQTL mapping, we embedded `sQTLseeker2` in a Nextflow²³ (plus
52 Docker, <https://www.docker.com/>) computational workflow named `sqt1seeker2-nf`, available at
53 <https://github.com/dgarrimarr/sqt1seeker2-nf>.

54 Here we extensively analyze the sQTLs identified by `sqt1seeker2-nf`, using the expression and
55 genotype data produced by the GTEx Consortium. For most of the analyses, we employed isoform quantifications
56 obtained from the V7 release (dbGaP accession *phs000424.v7.p2*), corresponding to 10,361 samples from 53 tissues of 620 deceased donors. 48 tissues with sample size ≥ 70 were selected for sQTL
57 analyses. We tested variants in a *cis* window defined as the gene body plus 5 Kb upstream and downstream
58 the gene boundaries. In addition, to demonstrate that the statistical framework of `sQTLseeker2`
59 is not restricted to the analysis of transcript abundances, but it can leverage other splicing-related multi-
60 variate phenotypes, we have also computed the sQTLs based on the intron excision ratios obtained by
61 LeafCutter¹⁸ from the GTEx RNA-seq data (Supplementary Note 2). Finally, we also provide the sQTLs
62 identified by `sqt1seeker2-nf` in GTEx V8 (Supplementary Note 3), which can be compared to the sQTLs
63 produced by the GTEx Consortium in an upcoming publication¹².

64 At a 0.05 false discovery rate (FDR), we found in GTEx V7 a total of 210,485 *cis* sQTLs affecting 6,963 genes (6,685 protein coding genes and 278 long intergenic non-coding RNAs, lincRNAs). On average, per tissue, we identified 1,158 sGenes (Table S1). 44% and 34% of all tested protein coding genes and lincRNAs, respectively, were found to be sGenes. In an analogous experimental setting, the GTEx Consortium reported genetic variants affecting expression (expression QTLs, eQTLs) for 95% and 71% of all tested protein coding genes and lincRNAs, respectively²⁴. To illustrate the nature of the sQTLs identified with `sqt1seeker2-nf`, in Fig. 1 we show the example of the SNP rs2295682, an sQTL for the gene RBM23 shared across 46 tissues, with larger effect in brain subregions such as cortex. The SNP strongly

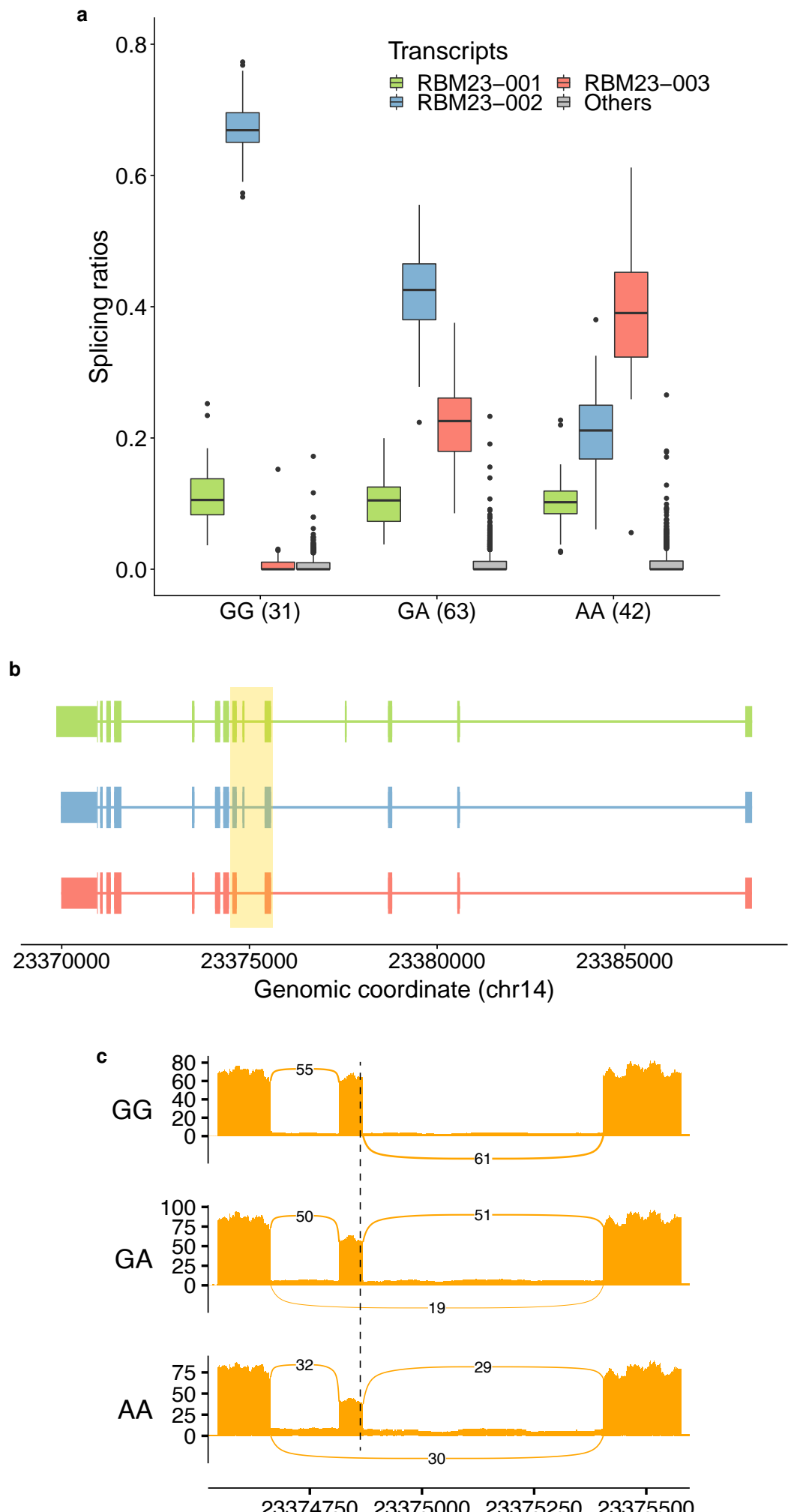


Figure 1

sQTL example. **a)** Relative abundances of the three most expressed isoforms in the brain cortex from the gene RBM23 (chr14:23,369,854-23,388,393, reverse strand, RBM23-001, RBM23-002 and RBM23-003, all protein coding), for each genotype group at the rs2295682 locus (chr14:23,374,862, G/A in the reverse strand). RBM23 encodes for an RNA-binding protein that may be itself involved in splicing. The least abundant isoforms are grouped in *Others*. The number of individuals in each genotype group is shown between parentheses. Individuals that are homozygous for the reference allele (GG) at the SNP locus, express preferentially RBM23-002 (blue), while they barely express RBM23-003 (red). In contrast, AA homozygous express preferentially RBM23-003 (red). Heterozygous individuals exhibit intermediate abundances. RBM23-001 (green) has similar levels in the three genotype groups. **b)** Exonic structure of the isoforms and location of exons 5, 6 and 7 (highlighted area). Compared to RBM23-001 (green), RBM23-002 (blue) lacks exon 6, and RBM23-003 (red), exons 4 and 6. **c)** Sashimi plot (corresponding to the highlighted area in b) displaying the mean exon inclusion of exon 6 of RBM23 across all brain cortex samples of each genotype group at rs2295682, obtained by `ggsashimi`⁸⁴. The dashed line marks the location of the SNP. The number of reads supporting exon skipping increases with the number of copies of the alternative allele A, matching the changes observed in isoform abundances. This allele has been previously associated with increased skipping of exon 6⁸⁵.

73 affects the relative abundances of the AS isoforms of the target gene, the dominant isoform depending on
74 the genotype at the sQTL.

75 As expected, the number of sGenes over the number of tested genes grows with the tissue sample size
76 ($r^2 = 0.91$). This is explained by the gain of power to detect sQTLs as the number of samples increases
77 (Fig. 2a). No signs of saturation are observed. Some tissues, such as skeletal muscle or whole blood (with
78 less sQTLs than expected) and testis (with more sQTLs than expected) escape the general trend. This was
79 also observed for eQTLs²⁴. The cell type heterogeneity of the tissue, estimated using xCell²⁵, does not
80 seem to have a large impact on sQTL discovery compared to the tissue sample size (the partial correlation
81 between the number of sGenes over the number of tested genes and the estimated cell type heterogeneity,
82 controlling for the tissue sample size, is 0.23, *p* value 0.11, see Methods).

83 sQTL effect sizes, measured as the absolute maximum difference (MD) in adjusted transcript relative
84 expression between genotype groups (see Methods), are generally low to moderate (MD from 0.05 to
85 0.20). Nevertheless, around 20% of sQTLs account for large effects (MD ≥ 0.20). As one would expect,
86 the median effect size detected across tissues drops substantially with increasing sample sizes (Fig. S1),
87 given that larger sample sizes allow the detection of smaller effects. Fig. 2b represents sQTL effect
88 sizes (MD values) *vs p* values, together with the distribution of the former, for tibial artery ($n = 388$) and
89 hypothalamus ($n = 108$).

90 GO enrichment analysis of sGenes shows a wide variety of biological processes, including cellular
91 transport, immune response, mitochondrial functions and, interestingly, RNA processing (Fig. S2a). This
92 might suggest some mechanism of splicing autoregulation, as it has been previously described²⁶. In con-
93 trast, tested genes without sQTLs are enriched in functions related to signaling and, especially, develop-
94 ment (Fig. S2b). This resembles the behaviour reported for genes without eQTLs²⁴, as it does the fact that
95 genes without sQTLs are less expressed than sGenes in all tissues (Wilcoxon Rank-Sum test *p* value <
96 10^{-16}).

97 The sQTLs found here are highly replicated in other studies. We compared them with those obtained
98 in the Blueprint Project²⁷ for three major human blood cell types (CD14⁺ monocytes, CD16⁺ neutrophils,
99 and naive CD4⁺ T cells, see Methods). The majority of GTEx sQTLs replicate at 5% FDR (from $\pi_1 = 0.80$
100 in brain subregions to $\pi_1 = 0.96$ in whole blood). As expected, whole blood displays the highest sQTL
101 replication rate (Fig. S3).

102 We characterized the types of alternative splicing (AS) events associated with sQTLs (see Methods,
103 Fig. S4a). Note that here we also account for other relevant sources of transcript diversity, such as alter-
104 native transcription initiation and termination²⁸. sQTLs generally involve multiple events (on average 2.63).
105 Around 34% of sQTLs are related to at least one AS event involving internal exons and/or introns. Among
106 them, exon skipping is the most frequent simple event (7% to 10% of all events). In addition, 58% of sQTLs
107 are associated with events affecting first/last exons and untranslated regions (UTRs). The landscape of
108 AS events associated with sQTLs is very similar across tissues. However, brain subregions present some
109 particularities when compared to non-brain tissues, such as a larger proportion of exon skipping events

Figure 2

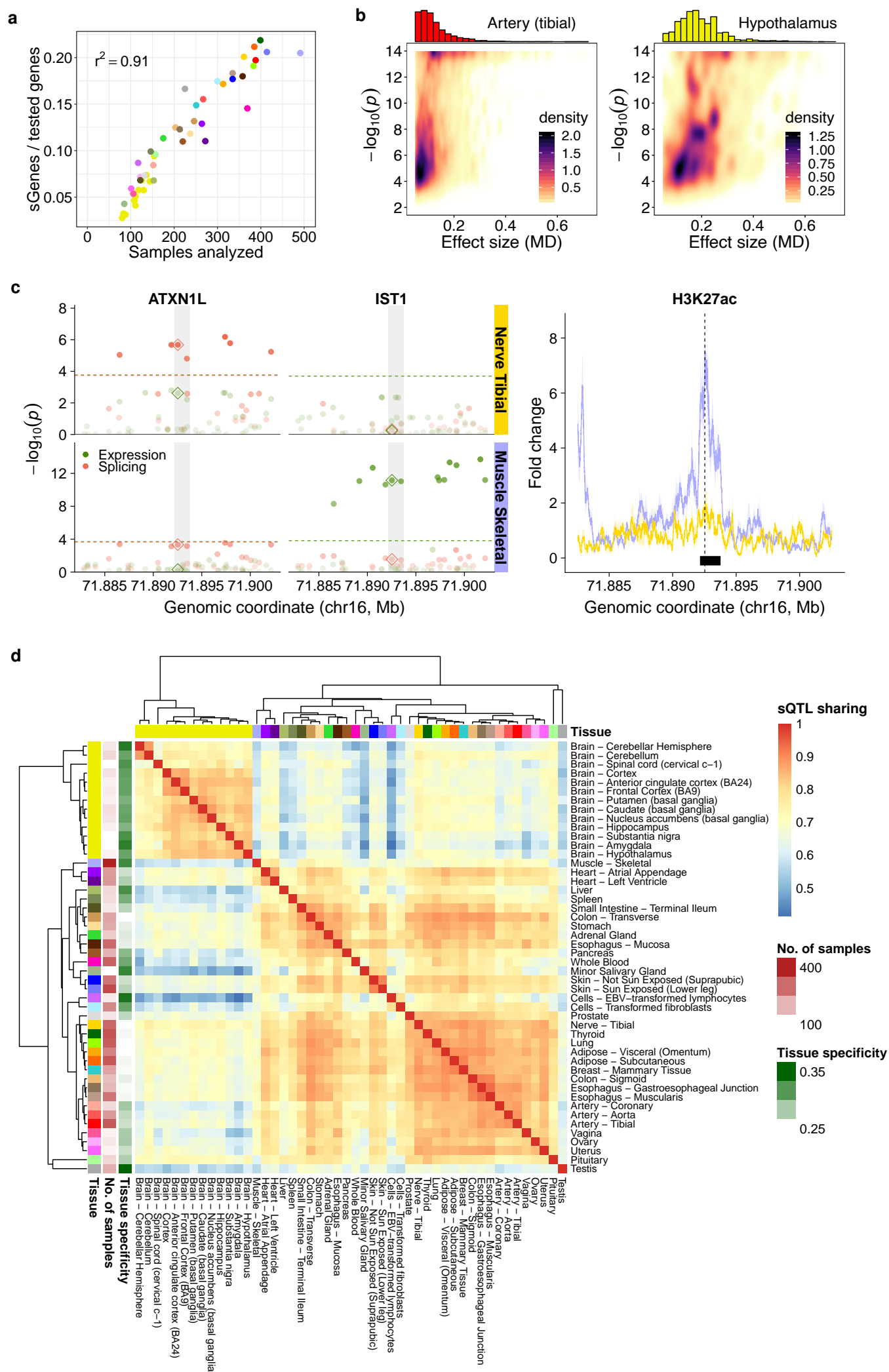


Figure 2

Overall results, heteropletropy and sQTL sharing across tissues. **a)** Proportion of sGenes (over tested genes) per tissue (y-axis) with respect to the tissue sample size (x-axis). Tissue color codes are shown in Table S1. **b)** For two tissues with markedly different sample sizes, such as tibial artery (upper panel, 388 samples) and hypothalamus (lower panel, 108 samples), we display the effect sizes (MD values, x-axis) of significant sQTLs *vs* the $-\log_{10}$ of their association p value with the target sGene (y-axis). The density of points is shown, together with the sQTL effect size distribution. Note that MD for sQTLs is bounded to [0.05, 1] (see Methods). **c)** Example of an heteropletropic locus. The SNP rs8046859 (chr16:71,892,531, C/T), an sQTL for the gene ATXN1L (chr16:71,879,894-71,919,171, forward strand) in Nerve Tibial, but not in Muscle Skeletal. The SNP is not an eQTL for ATXN1 in any of the two tissues. In contrast, the SNP is an eQTL for the gene IST1 (chr16:71,879,899-71,962,913, forward strand) in Muscle Skeletal, but not in Nerve Tibial. The SNP is not an sQTL for IST1 in any of the two tissues. In the left panel, the dots represent the $-\log_{10} p$ values of association with the expression (green) and splicing (red) of the two genes in the two tissues, for variants in a 20Kb window centered at rs8046859 (the $-\log_{10} p$ values corresponding to rs8046859 are highlighted by a diamond). The transparency of the dots depends on the $-\log_{10} p$ value. The significance level for each molecular trait, gene and tissue is shown as a colored, dashed horizontal line. When this line is not present, the gene-level p value is above the 0.05 FDR threshold and hence no variant is significantly associated with this molecular trait in this tissue (see Methods). The shaded area represents the position of a H3K27ac ChIP-seq peak (see below). The right panel shows the fold-change signal of the H3K27ac histone mark with respect to the input across ENTEEx donors in Nerve Tibial and Muscle Skeletal, in the same genomic region of the left panel. The solid line and coloured area correspond to the mean signal and its standard error across 4 ENTEEx donors, respectively. The location of the SNP and the overlapping ChIP-seq peak (intersection of the peaks in the 4 donors) are also displayed. **d)** Heatmap of sQTL sharing across GTEx tissues. Sharing estimates (see Methods) range from 0 (low sharing, blue) to 1 (high sharing, red). In addition, hierarchical clustering of the tissues based on sQTL sharing is displayed, together with the tissue sample sizes and tissue specificity estimates.

110 and a smaller proportion of complex events involving the 3' gene terminus (see Fig. S4b,c for details).

111 We found that 52% of the identified sQTLs are also eQTLs for the same gene and tissue, although the
112 top sQTL coincides with the top eQTL only in 3% of the cases. This relatively large overlap, which departs
113 from that reported in some previous studies¹⁵, matches what was observed for sQTLseekeR sQTLs in the
114 GTEx pilot²⁹. This is partially due to our sQTLs being able to involve transcriptional termini, in addition to
115 canonical splicing events. It also indicates a substantial degree of co-regulation of gene expression and
116 splicing, either at the level of transcription (e.g. variants that impact transcription and thus, splicing), or at
117 the level of transcript stability (e.g. variants that affect splicing, and as a consequence, transcript stability
118 and gene expression).

119 We focused on a set of 148,618 variants that were tested for association with both the expression
120 and splicing of two genes (i.e. g_1 and g_2) or more, in at least two tissues, and identified 6,552 cases
121 in which the variant is only sQTL for gene g_1 , but not for gene g_2 , in one tissue, and it is only eQTL for
122 gene g_2 , but not for gene g_1 , in a different tissue (Fig. S5a). These cases uncover regulatory loci in
123 the genome that, either through the same causal variant or through different causal variants in linkage
124 disequilibrium (LD), have different effects on different genes through likely different molecular mechanisms.
125 We term this phenomenon *heteropleiotropy*. We found evidence supporting the dual regulatory behaviour of
126 heteropleiotropic loci. We identified the ChIP-seq peaks corresponding to six histone modifications from the
127 ENTEX Project overlapping the heteropleiotropic variants above (see Methods). We hypothesized that loci
128 with different regulatory effects (i.e. splicing and expression) in different tissues would be differently marked
129 by histone modifications in these tissues. Indeed, we observed histone modification changes in 24% of the
130 heteropleiotropic variants (Table S2), compared to 19% of non-heteropleiotropic variants (Fisher's exact
131 test test p value 0.045, see Methods). Regardless of the underlying causal structure, heteropleiotropic
132 loci would uncover genomic regions that allow the coordinated regulation of different processes and affect
133 different genes which otherwise do not appear to interact directly with each other. While further work is
134 required to establish the relevance and generality of this phenomenon, figures 2c and S5b show some
135 potentially interesting examples.

136 sQTLs are highly shared across tissues

137 The large number of tissues available in GTEx allowed us to evaluate tissue sharing and specificity of
138 sQTLs. For every pair of tissues, we selected variant-gene pairs tested in both and found significant in at
139 least one, and computed the *Pearson* correlation (r) between their effect sizes (MD values). Hierarchical
140 clustering based on these correlations grouped tissues with similar sQTL sharing patterns (Fig. 2d). A
141 comparable clustering was obtained when using the more stringent *Jaccard* index (Fig. S6). Brain sub-
142 regions cluster together and apart from the rest of the tissues, which form a second major cluster. We
143 observe a high degree of sQTL sharing within each of the two groups ($\bar{r} = 0.80$ and 0.78, respectively),
144 but lower between them ($\bar{r} = 0.64$). The same pattern was depicted for eQTLs in GTEx²⁴. We further
145 estimated tissue specificity as $s_t = 1 - \bar{r}_t$, where \bar{r}_t is the mean correlation between a given tissue t and the

146 others (tissue specificity estimates shown in Fig. 2d). On average, brain sQTLs are more tissue-specific
147 than non-brain sQTLs ($\bar{s}_t = 0.31$ vs 0.25, Wilcoxon Rank-Sum test p value $9.32 \cdot 10^{-5}$). Other tissues with
148 relatively high tissue-specific sQTLs include testis (0.37), skeletal muscle (0.33) or liver (0.32).

149 sQTLs with large effects are more shared than those with smaller effects (Fig. S7a). As with eQTLs²⁴,
150 the detection of sQTLs with small effects requires larger sample sizes, thus sQTLs in tissues with small
151 sample sizes tend to be more shared, while sQTLs identified in tissues with large sample sizes tend to be
152 more tissue-specific (Fig. S7b). To rule out an effect of the sample size in the patterns of sQTL sharing,
153 we downsampled the original dataset to 100, 200 and 300 samples per tissue, and evaluated again sQTL
154 sharing. We found that the patterns of sQTL sharing above are replicated independently of the sample size
155 (Fig. S8).

156 To capture more complex sharing patterns, we further designed a geometric approach that compares
157 changes in the whole splicing phenotype due to sQTLs between tissues (see Methods and Fig. S9a).
158 The derived tissue dendrogram (Fig. S9b) displayed high similarity with the ones generated by simpler
159 approaches (i.e. based on MD values and *Jaccard* index), and also with the one obtained using *multivariate*
160 *adaptive shrinkage*³⁰ on LeafCutter sQTLs from GTEx V8¹² (Fig. S9c). This strongly supports the
161 robustness of the sQTL sharing patterns observed.

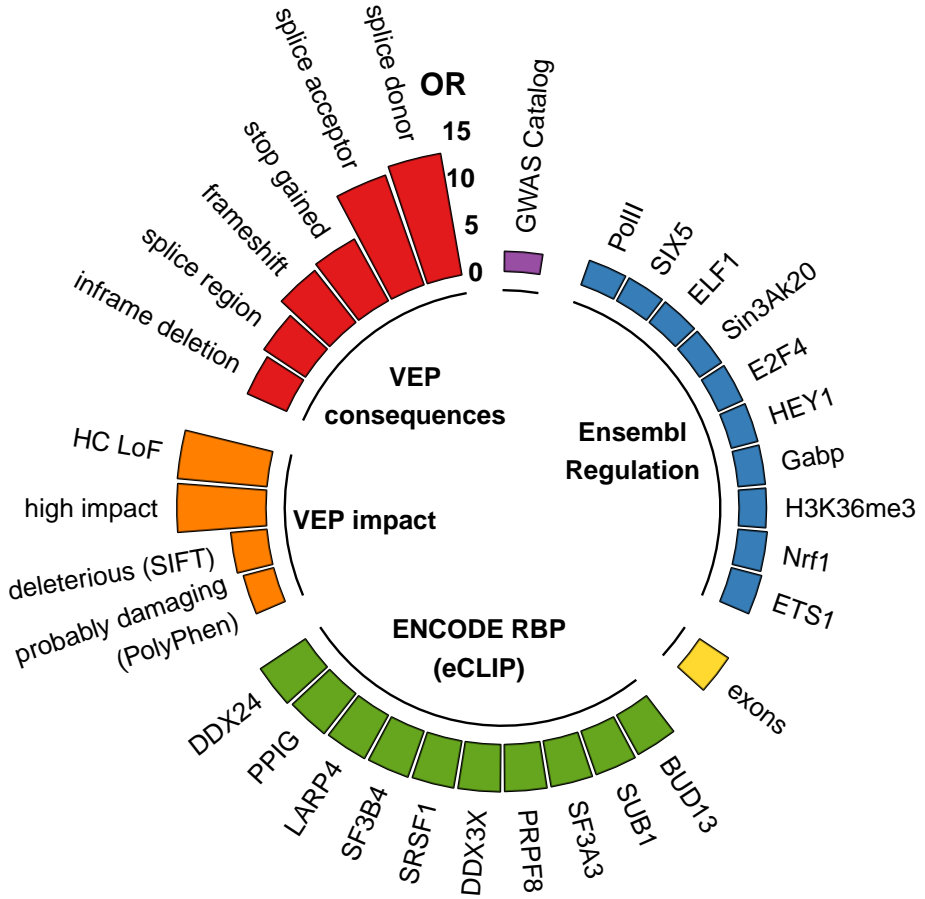
162 sGenes are also markedly shared: 66% of genes tested in all tissues are sGenes in at least two tis-
163 sues. To identify tissue-specific sGenes, we computed τ_s , a variation of the τ index³¹ based on sGene
164 significance. We also employed the standard τ to determine the tissue specificity of sGene expression
165 (see Methods). We found 469 genes under strong tissue-specific splicing regulation (highly tissue-specific
166 sGenes), 81 of which did not display tissue-specific expression (Table S3). GO enrichment of these genes
167 (universe: all sGenes) identified biological processes related to RNA processing and its regulation (three
168 out of all five significant terms at FDR < 0.1: *RNA splicing via transesterification reactions, regulation of*
169 *RNA splicing, regulation of mRNA processing*) suggesting again some mechanism of splicing autoregula-
170 tion²⁶.

171 **sQTLs are enriched in functional elements of the genome related to splicing and in high- 172 impact variants**

173 To shed light on the mechanisms through which sQTLs may impact splicing, we built a comprehensive func-
174 tional annotation of the human genome (see Methods). Overall, we observed a high density of functional
175 elements in the proximity of sQTLs (Fig. S10). We next evaluated the enrichment of sQTLs in every func-
176 tional category, with respect to a null distribution of similar variants not associated with splicing (Fisher's
177 exact test, FDR < 0.05). The top enrichments are summarized in Fig. 3a (the complete list, together with
178 the statistical significance associated with each enrichment, is shown in Fig. S11).

179 As one would expect from *bona fide* variants affecting splicing, sQTLs are strongly enriched in splice
180 sites (donors: OR = 12.98, adj. p value $< 10^{-16}$; acceptors: OR = 12.23, adj. p value $1.22 \cdot 10^{-15}$). They
181 also display enrichments in exons, transcription factor (both activator and repressor) binding sites, RNA

a



b

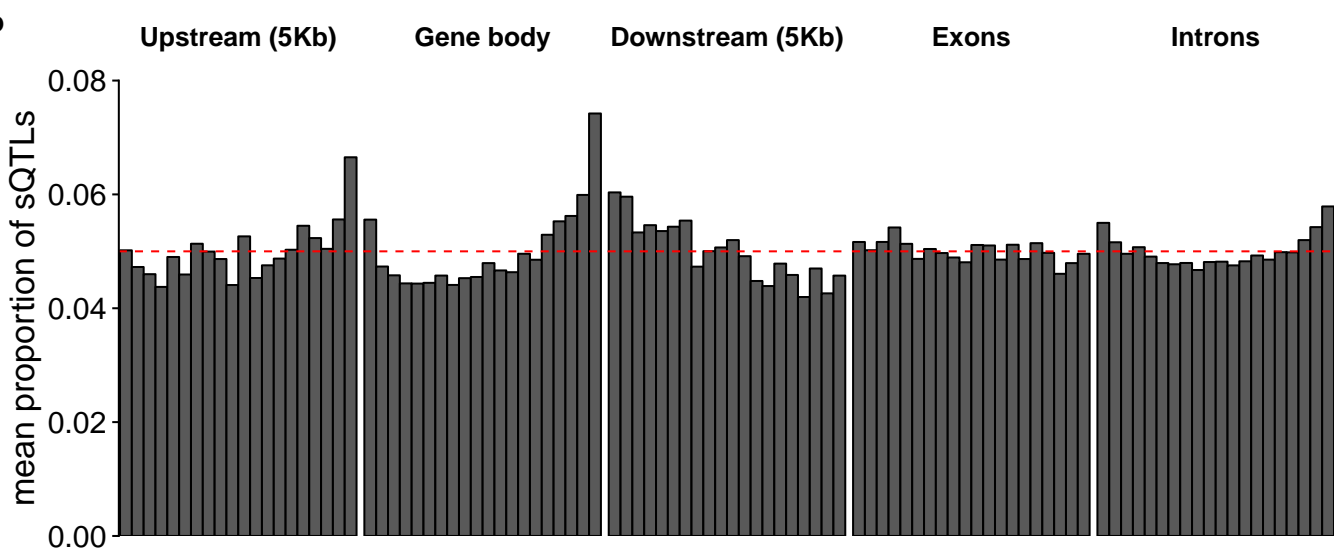


Figure 3

Functional enrichment and distribution of sQTLs. **a)** Top enrichments of sQTLs in functional annotations. The height of the bars represents the odds-ratio (OR) of the observed number of sQTLs to the expected number of variants that are not sQTLs overlapping a given annotation (see Methods): Variant Effect Predictor (VEP) categories (red) and impact (orange), ENCODE RNA-binding proteins (RBPs) eCLIP peaks (green), exons of GENCODE v19 protein coding and lincRNA genes (yellow), Ensembl Regulatory Build elements (blue) and GWAS catalog hits (purple). All these enrichments are significant at $\text{FDR} < 0.05$ and have OR confidence intervals not overlapping the range $[1/1.50, 1.50]$. **b)** Distribution of the mean proportion of sQTLs along the gene bodies of sGenes, their upstream and downstream regions, introns and exons. The red dashed line represents the expected distribution under a uniform model (see Methods).

182 binding protein (RBP) binding sites, including several relevant splicing factors and spliceosomal compo-
183 nents, and RNA Pol II sites. sQTLs tend to fall in open chromatin regions and show enrichments for several
184 chromatin marks, particularly for H3K36me3 (OR = 2.85, adj. p value $< 10^{-16}$). H3K27me3 regions, in
185 contrast, are depleted of sQTLs (OR = 0.63, adj. p value $< 10^{-16}$). sQTLs display large enrichments in
186 predicted protein loss-of-function consequences (stop-gained, frameshift, VEP high impact variants, LOF-
187 TEE high-confidence loss-of function variants (HC-LoF)) and potentially deleterious variants (according to
188 Polyphen³² and SIFT³³ scores). In addition, we found an enrichment in variants in high LD ($r^2 \geq 0.80$) with
189 GWAS hits (OR = 2.08, adj. p value $< 10^{-16}$). When performing stratified enrichments (see Methods), we
190 found that large effect size sQTLs are more enriched in high impact variants, splice sites and GWAS hits,
191 while small effect size sQTLs show larger enrichments in RBP binding sites, TFBS and open chromatin
192 regions (Fig. S12).

193 In contrast to eQTLs, which tend to cluster around transcription start sites (TSS)^{7,24}, we found sQTLs
194 preferentially located towards transcription termination sites (TTS) (Fig. 3b), as previously observed¹⁵.
195 In addition, while exonic sQTLs are uniformly distributed, intronic sQTLs are biased towards splice sites.
196 Overall, sQTLs are closer to splice sites than non-sQTLs (Wilcoxon Rank-Sum test p value $< 10^{-16}$, Fig.
197 S13).

198 **sQTLs affect splice site strength and RNA-binding protein (RBP) binding**

199 Enrichments in functional annotations (Fig. 3a) suggested several mechanisms through which sQTLs may
200 affect splicing. One of them is the modification of splice site strength. Thus, for each variant within the
201 sequence of an annotated splice site, we scored the site considering the reference and the alternative
202 allele, using position weight matrices (see Methods). Overall, when compared to non-sQTL variants, a
203 larger fraction of sQTLs modifies splice site strength (63% vs 49%, OR = 1.79, Fisher's exact test p value
204 $< 10^{-16}$). The absolute difference in splice site strength is also larger for sQTLs (Wilcoxon Rank-Sum test
205 p value $1.98 \cdot 10^{-7}$), and increases with the sQTL effect size (Fig. 4a).

206 Another mechanism through which sQTLs may affect splicing is the modification of RNA-binding protein
207 (RBP) binding sites. To investigate it, we used eCLIP peaks of 114 RBPs available for HepG2 and K562
208 cell lines from the ENCODE project³⁴. We employed a k-mer-based machine learning approach, which
209 has been shown to outperform PWMs to identify transcription factor binding sites³⁵ and provides a unique
210 framework to assess the impact of genetic variants on the binding³⁶. First we trained, for each RBP, a
211 gapped k-mer support vector machine (gkm-SVM)³⁷ on the sequences of high-confidence eCLIP peaks.
212 79 RBPs with a mean cross-validation ROC AUC ≥ 0.8 were kept. Then, we estimated the impact of all
213 variants (whether sQTLs or not) overlapping the eCLIP peaks of each of these RBPs via the deltaSVM
214 metric³⁶, which measures the difference in predictive potential between the variant alleles (see Methods).
215 To ensure the robustness of our results, we further restricted the analysis to RBPs with at least 30 sQTLs
216 among the top 5% variants most predictive of the binding of the RBP at either allele, resulting in a final set
217 of 32 RBPs (see Methods).

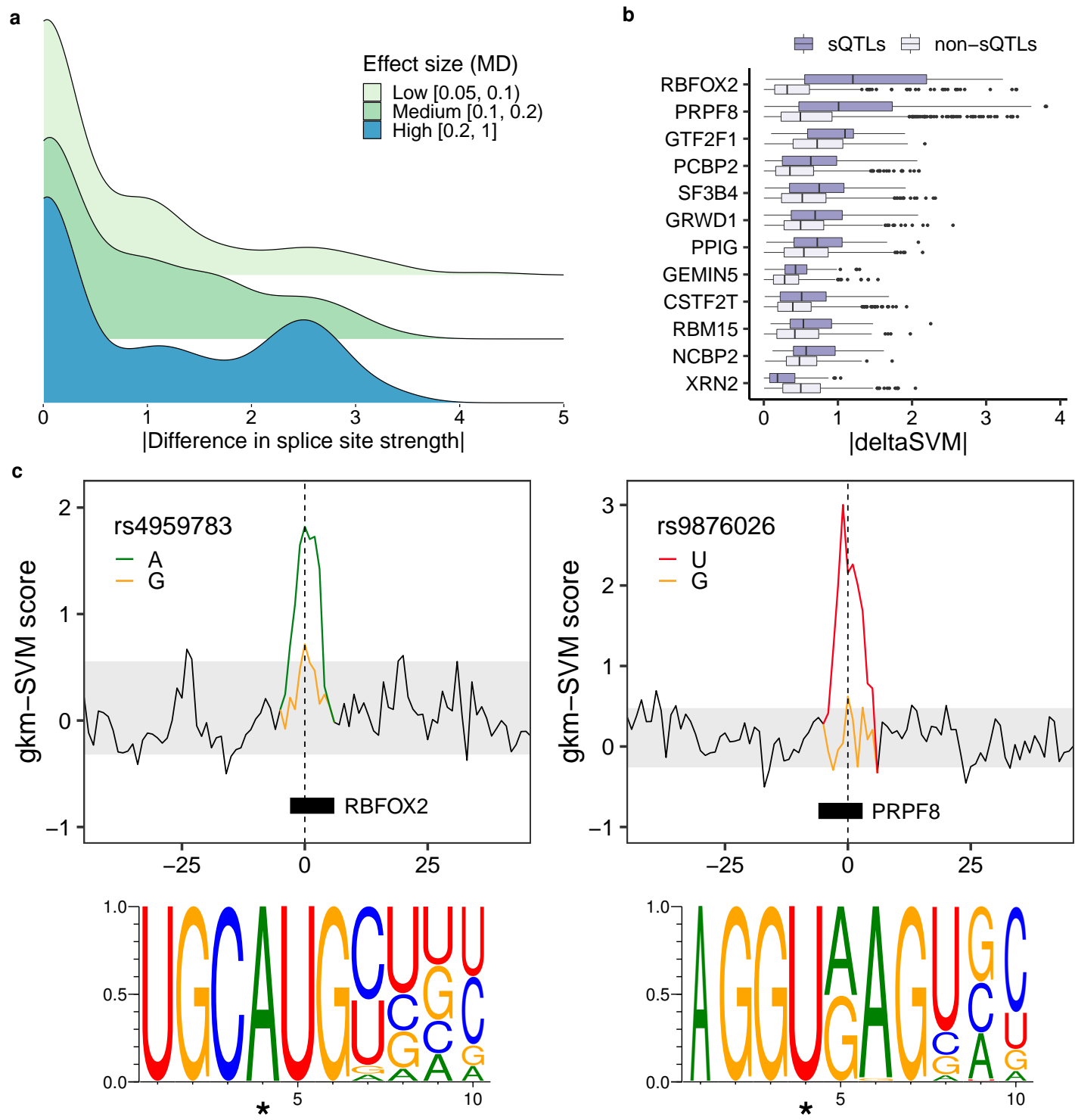


Figure 4

Impact of sQTLs on splice sites and RBP binding sites. **a)** Distribution of the absolute change in splice site strength for sQTLs with low, moderate and high effect sizes (MD value). **b)** Distribution of the absolute deltaSVM value ($|\delta\text{SVM}|$) of sQTLs and non-sQTLs, for RBPs with significantly different mean $|\delta\text{SVM}|$ between sQTLs and non-sQTLs ($\text{FDR} < 0.1$). **c)** Modification of the binding sites of the RBPs RBFOX2 (left) and PRPF8 (right) by SNPs rs4959783 (chr6:3,260,093, G/A, $|\delta\text{SVM}| = 2.48$) and rs9876026 (chr3:11,849,807, T/G in the reverse strand, $|\delta\text{SVM}| = 4.77$), respectively. The lines represent the gkm-SVM scores of all possible (overlapping) 10-mers in a 100bp window around the SNP. Those corresponding to the 10-mers overlapping the SNP are colored according to the allele. SNP positions are marked with a dashed line. The grey area includes the 90% middle gkm-SVM scores of 10-mers not overlapping the variant. The relative location of the predicted RBP motifs and the corresponding sequence logos are also displayed. In the logos, the SNP position is marked with an asterisk.

218 At FDR < 0.1, differences in $|\delta\text{SVM}|$ between sQTLs and non-sQTLs were found significant for
219 12 RBPs (Fig 4b, the corresponding gkm-SVM ROC curves and motif logos shown in figures S14 and
220 S15, respectively). Notably, for 11 of these proteins the $|\delta\text{SVM}|$ values are larger for sQTLs than for
221 non-sQTLs, as expected from variants regulating splicing. In addition, three of them (PPIG, SF3B4 and
222 PRPF8) are among the top 10 RBPs whose binding sites are more enriched in sQTLs (Fig. 3a). In Fig. 4c,
223 we show examples of the impact of the SNPs rs4959783 and rs9876026, which are sQTLs for the genes
224 PSMG4 and TAMM41 (see also Fig. S16) and disrupt the binding sites of the RBPs RBFOX2 and PRPF8,
225 respectively.

226 We further investigated whether allele-specific RBP binding (ASB) was occurring specifically at sQTLs.
227 We obtained a set of ASB variants identified in the ENCODE eCLIP dataset using BEAPR (Binding Estima-
228 tion of Allele-specific Protein-RNA interaction)³⁸ and overlapped them with our sQTLs (see Methods). We
229 found that sQTLs were highly enriched in ASB variants, when compared to non-sQTLs, across all RBPs
230 (OR = 2.30, Fisher's exact test p value < 10^{-16}). When considering individual RBPs, at FDR < 0.05 we
231 found a significant enrichment of sQTLs among ASB variants for 22 of them (Fig. S17), including 7 of
232 the ones identified above with larger $|\delta\text{SVM}|$ values for sQTLs. Altogether, these results suggest that
233 sQTLs may affect splicing through allele-specific binding of RBPs.

234 Overall, the effect sizes (MD) of sQTLs in splice sites are larger than those of sQTLs overlapping RBP
235 eCLIP peaks (Wilcoxon Rank-Sum test p value $1.98 \cdot 10^{-7}$, Fig. S18), although the proportion of sQTLs in
236 splice sites is much smaller (1.5% vs 8.3% out of all sQTLs). Often, both mechanisms may co-occur, as
237 many RBPs bind near splice sites. This is the case of PRPF8, which binds specifically to the sequence of
238 splice donors³⁹. Indeed, the SNP rs9876026 (Fig. 4c), which modifies $|\delta\text{SVM}|$ and has been identified
239 as an allele-specific binding SNP for PRPF8 by BEAPR, also disrupts a donor splice site.

240 sQTLs are preferentially located on post-transcriptionally spliced introns

241 Although splicing generally occurs co-transcriptionally (most introns are spliced prior to transcription ter-
242 mination and polyadenylation), there is a group of transcripts, often alternatively spliced, that tend to be
243 processed more slowly, even post-transcriptionally⁴⁰. We evaluated the role of genetic variants in the reg-
244 ulation of co- and post-transcriptional splicing (here referred to as *cs* and *ps*, respectively). In order to
245 identify *cs* and *ps* introns, we determined the degree of splicing completion of annotated introns in nuclear
246 and cytosolic RNA-seq data available for 13 cell lines from the ENCODE project (see Methods). We fo-
247 cused on a subset of introns consistently classified as either *cs* or *ps* in at least 10 of the analyzed cell lines
248 (14,699 and 6,419 introns, respectively).

249 We observe a higher variant density in *ps* introns than in *cs* introns (4.38 vs 3.34 variants/Kb, differently
250 distributed along the intron, Fig. S19a). The proportion of variants that are sQTLs in *ps* introns is larger than
251 in *cs* introns (9.2% compared to 6.6%, OR = 1.47, Fisher's exact test p value < 10^{-16}). This enrichment
252 is stronger when considering sQTLs that are not eQTLs for the same gene and tissue (OR = 1.67, p value
253 < 10^{-16}). Furthermore, sQTLs in *ps* introns display a substantial enrichment, with respect to sQTLs in

254 cs introns, in RBPs and Pol II binding sites, and less markedly, in histone marks such as H3K36me3 and
255 H3K4me3, open chromatin regions and TFBS (Fig. S19b). The proportion of sQTLs overlapping splice
256 sites and GWAS hits is not significantly different between the two types of introns.

257 These results suggest that splicing regulation occurs preferentially at *ps* introns. This is expected, since
258 these introns are retained longer within the primary transcript, offering more opportunities for regulation
259 through the interaction with RBPs and other factors, including chromatin-related ones.

260 **sQTLs help to gain insight into disease and complex traits**

261 To explore the relevance of regulatory variation affecting splicing in disease and complex traits, we as-
262 sessed the overlap between GTEx sQTLs and the GWAS Catalog (<https://www.ebi.ac.uk/gwas/>),
263 extended to include variants in high LD ($r^2 \geq 0.80$) with the GWAS hits. sQTLs display a substantial en-
264 richment, when compared to non-sQTLs, in variants associated with a wide variety of GWAS traits and
265 diseases (median OR = 3.23). Among the diseases with the largest sQTL enrichment, we find many for
266 which alternative splicing has been previously related to their pathophysiology (Table S4). We integrated
267 the enrichment information with estimates of semantic similarity between individual GWAS terms, com-
268 puted from the Experimental Factor Ontology (EFO)⁴¹. Then, we applied multidimensional scaling (MDS)
269 to summarize and represent the results (see Methods). This allowed us to identify the major phenotype
270 groups related to sQTLs. Trait measurements (right-hand side of the MDS plot) and diseases (left-hand
271 side) are the two main groups of enriched GWAS terms observed (Fig. 5a). Within the latter, we identify
272 subgroups corresponding to cancer, autoimmune diseases and other disorders (neurological, cardiovascu-
273 lar, metabolic, etc.).

274 We also compiled genome-wide GWAS summary statistics for a subset of enriched traits representative
275 of the observed clusters: asthma⁴², breast cancer⁴³, coronary artery disease⁴⁴, heart rate⁴⁵, height⁴⁶, LDL
276 cholesterol levels⁴⁷, rheumatoid arthritis⁴⁸ and schizophrenia⁴⁹. Overall, sQTLs show stronger GWAS
277 associations than non-sQTL variants (Fig. S20). We further characterized the contribution to the disease
278 phenotype of variants affecting splicing and variants affecting exclusively gene expression using *fgwas*⁵⁰
279 (see Methods). For most of the traits analyzed, including asthma, breast cancer, coronary artery disease,
280 heart rate, height and rheumatoid arthritis, we observe stronger effects among variants affecting splicing
281 than among variants affecting only gene expression (Fig. 5b), suggesting that alterations in splicing play
282 a relevant role in the molecular mechanisms underlying these traits. A few others, such as LDL levels
283 or schizophrenia, display the opposite behaviour, pointing to a predominant effect of alterations in gene
284 expression in the disease phenotype.

285 In addition, we observe that GWAS variants are especially enriched among sQTLs located in splice
286 sites (OR = 2.66, Fisher's exact test *p* value $1.02 \cdot 10^{-9}$) or within RBP binding sites (OR = 1.78, Fisher's
287 exact test *p* value $< 10^{-16}$). In particular, some of the traits and diseases with available summary statis-
288 tics analyzed display stronger GWAS associations for sQTLs in RBP binding sites than for other sQTLs.
289 Notably, this behaviour seems trait/disease and RBP-specific (Fig. S21).

Figure 3

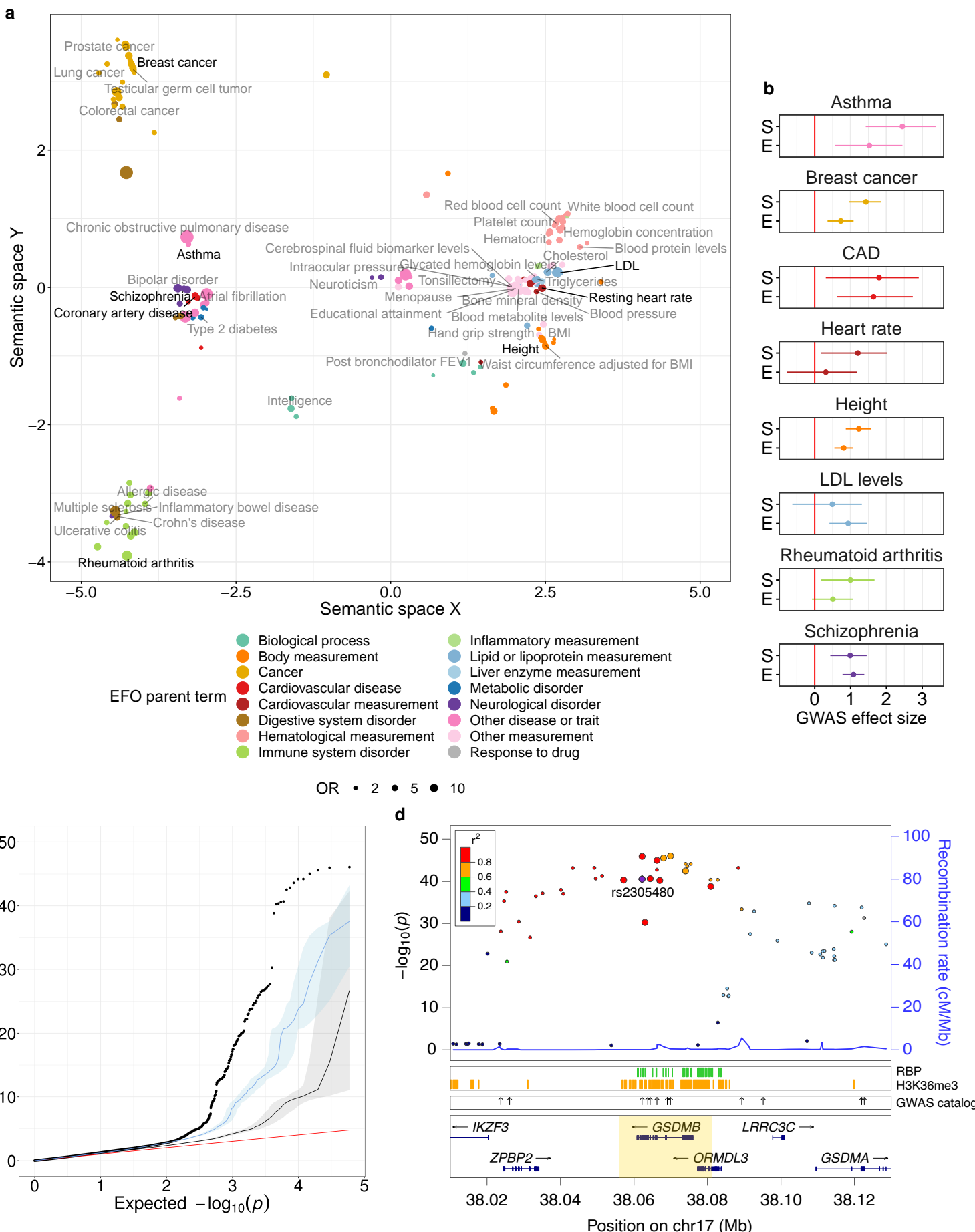


Figure 5

sQTLs and GWAS. **a)** Multidimensional scaling-based representation of the semantic dissimilarities between GWAS traits and diseases whose associated variants are enriched among sQTLs with respect to non-sQTLs ($FDR < 0.05$). Each GWAS term is represented by a dot, whose size corresponds to the enrichment odds-ratio (OR), and the color to the Experimental Factor Ontology (EFO) parent category the term belongs to. GWAS terms that lie close to each other are semantically similar. Eight representative traits with available summary statistics are highlighted. To help visualization, only the labels for the non-redundant, confidently and highly enriched terms are displayed (p value $< 10^{-8}$, lower bound of the 95% confidence interval (CI) for the OR estimate > 1.5 , width of the 95% CI for the OR estimate below the median). **b)** Maximum likelihood estimates and 95% CIs for the GWAS association effect size of variants affecting splicing (S) and expression, but not splicing (E), for eight traits and diseases. **c)** Quantile-quantile plot of p values for association with asthma in Demenais *et al.*⁴² for sQTLs (black dots), eQTLs without effects on splicing (blue), and variants with effects neither on expression nor on splicing (grey). Solid lines and coloured areas represent means and 95% CIs across 10,000 random samplings, respectively. The identity line is shown in red. **d)** p values for association with asthma in Demenais *et al.*⁴² (left y-axis) of variants in the region chr17:38,010,000-38,130,000, around the GSDMB gene (highlighted). The larger dots correspond to variants identified as sQTLs for the GSDMB gene in the lung. Linkage disequilibrium patterns (color-coded) and recombination rates are also displayed. The lower panels represent the location of RNA-binding protein (RBP) eCLIP peaks, H3K36me3 marked-regions and other GWAS-catalog associations with asthma (shown as arrows). The highlighted variant (rs2305480) is in perfect LD with rs11078928, previously shown to have an impact in GSDMB splicing⁵⁴.

290 An interesting example of how sQTL mapping can help to gain insight into the mechanisms underlying
291 GWAS associations is the case of asthma and the gene *gasdermin b* (GSDMB). Asthma displays the
292 largest effect size for sQTL variants ($\bar{\beta} = 2.32$, Fig. 5b), and stronger associations for sQTLs than for
293 variants affecting only gene expression, or variants affecting neither expression nor splicing (Fig. 5c).
294 Indeed we identified over 850 sQTLs co-localizing with known asthma loci, affecting the splicing patterns of
295 genes related to immunity, including interleukins and immune cell's receptors (IL13, TLSP, IL1RL1, TLR1),
296 major histocompatibility complex components (HLA-DQA1, HLA-DQB1) or interferon-activated transcription
297 factors (IRF1). However we also found other genes, such as GSDMB, with *a priori* less clear roles in the
298 pathophysiology of the disease.

299 The GSDMB locus (17q21) has been consistently identified as a contributor to genetic susceptibility to
300 asthma⁴² and other autoimmune diseases, such as type 1 diabetes⁵¹, ulcerative colitis⁵² or rheumatoid
301 arthritis⁵³. Although its exact function is unknown, GSDMB is highly expressed in human bronchial epi-
302 thelial cells in asthma^{54,55}, and it is known that overexpression of the human GSDMB transgene in mice
303 induces an asthma phenotype⁵⁵. In addition, the lipid-binding N-terminal domain of GSDMB and other
304 gasdermins causes pyroptotic cell death⁵⁶, potentially leading to the release of inflammatory molecules
305 that trigger the asthma pathophysiology.

306 GSDMB is a sGene in 39 GTEx tissues, including lung (sGene FDR $1.42 \cdot 10^{-10}$, median MD 0.22).
307 Indeed, sQTLs for GSDMB are among the top associated variants with asthma in Demenais et al.⁴² (Fig.
308 5d). Allele C of the splice acceptor variant rs11078928 (chr17:38064469, T/C) has been shown to lead to
309 the skipping of exon 6, which encodes 13 amino acids in the N-terminal domain, disrupting its pyroptotic
310 activity⁵⁴. While the major allele (T) is associated with a higher incidence of asthma, the C allele confers
311 a lower asthma risk⁵⁴. We have identified rs11078928 as an sQTL for GSDMB, whose alternative allele
312 C precisely promotes expression of isoforms GSDMB-001 and GSDMB-002 (exon 6 skipping) vs isoform
313 GSDMB-003 (exon 6 inclusion) (Fig. S22).

314 Discussion

315 Using the unprecedented resource generated by the GTEx Consortium, we have obtained and analyzed
316 a comprehensive set of genetic variants in the human genome affecting transcript isoform abundances
317 (splicing QTLs, sQTLs). Unlike most methods for sQTL detection, we use a multivariate approach that
318 monitors global changes in the relative abundances of a gene's transcript isoforms, rather than targeting
319 specific splicing events. Leveraging the correlated structure of isoform abundances is likely to result in
320 increased power for sQTL mapping. Indeed, our approach has demonstrated the ability to detect sQTLs
321 associated with complex splicing events that often escape univariate approaches²⁰. In addition, we show
322 that our method is not restricted to the analysis of transcript abundances, but can also accommodate
323 other AS phenotypes, such as LeafCutter intron excision ratios¹⁸. A comparison of the resulting sQTLs
324 obtained employing the two types of input data highlights the complementarity between global and local

325 views of alternative splicing, especially regarding the types of splicing events identified^{20,29}.

326 We have surveyed a large collection of tissues. Our analyses show that sQTLs tend to be highly shared,
327 suggesting that there is a core set of variants that are involved in the regulation of splicing independently
328 of the tissue or cell type. This has also been recently reported by the GTEx Consortium¹². Among genes
329 whose splicing is regulated by genetic variants (i.e. sGenes), there is a consistent enrichment of functions
330 related to RNA processing, maybe reflecting splicing autoregulation. Indeed, several positive and negative
331 autoregulation and cross-regulation mechanisms, such as coupling to nonsense-mediated decay, have
332 been proposed for a large number of splicing factors²⁶.

333 Overall, we found fewer genes regulated at splicing than at expression level. This is in line with re-
334 cent reports¹², and with the smaller contribution of splicing, compared to gene expression, to the global
335 variability in transcript abundances across tissues and individuals^{57,58}. Many variants, however, seem to
336 be involved simultaneously in the regulation of both processes. This is not surprising, given that there is
337 a substantial interplay between the molecular mechanisms underlying splicing and transcription, and be-
338 cause splicing often takes place co-transcriptionally⁶. In addition, variants altering splicing can affect RNA
339 stability and, consequently, gene expression⁵⁹.

340 In this regard, we have observed that introns that are spliced post-transcriptionally (*ps*) tend to be more
341 enriched in sQTLs than introns that are spliced co-transcriptionally (*cs*). This is somehow expected, as *ps*
342 introns are retained longer within the primary transcript, offering more opportunities for regulation. Consis-
343 tent with this, sQTLs in *ps* introns display a larger enrichment, compared to sQTLs in *cs* introns, in RBP
344 binding sites, but also in Pol II binding sites and histone marks. We note that chromatin-related features
345 play a prominent role in co-transcriptional splicing, often through the regulation of transcription⁶. However,
346 not-fully spliced but already 3'-end mature transcripts are present in the fraction of RNA attached to chro-
347 matin^{60,61}. In this context, interactions between chromatin-side features and not-fully spliced transcripts
348 can occur post-transcriptionally. Indeed, similar enrichments have been reported for exons that are spliced
349 more slowly⁴⁰. Overall, it seems that post-transcriptionally spliced introns play a larger role in splicing
350 regulation than introns quickly spliced during transcription.

351 In addition to variants that are sQTLs and eQTLs for the same gene, we have found many variants that
352 are sQTLs for a gene and eQTLs for a different one. In order to rule out indirect regulatory effects (e.g.
353 when the variant directly affects the expression -splicing- of one gene, and the product of this gene directly
354 affects the splicing -expression- of the other gene), we considered each effect (splicing or expression)
355 occurring in different tissues, likely underestimating the number of such variants. Since our multivariate ap-
356 proach is not compatible with currently available co-localization methods (see below), we cannot distinguish
357 the cases in which the two effects are indeed caused by the same variant or by two different variants in
358 LD. Regardless of the underlying causal structure, these variants uncover regulatory loci, which we termed
359 heteropletotropic, that would be involved in the coordinated regulation, through different mechanisms, of
360 different genes which otherwise do not appear to directly interact. Thus, heteropletotropic loci could re-
361 veal regulatory relationships between genes that may not be easily captured by co-expression or splicing

362 networks, highlighting the complexity of the gene regulation program in eukaryotes. While further work is
363 required to establish the relevance and generality of this phenomenon, we believe that we have identified
364 a number of convincing examples.

365 Our study also helps to understand the molecular mechanisms through which genetic variants impact
366 splicing. Two such mechanisms appear to be the most relevant. On the one hand, direct impact on donor
367 and acceptor splice sites. On the other hand, modification of binding sites of a wide variety of transcriptional
368 regulators, especially RNA-binding proteins (RBPs), which are major players in RNA processing, transport
369 and stability^{5,62}. While the latter seems to occur in a larger number of cases, the former often leads to
370 stronger effects on splicing. However, in many cases both mechanisms are likely to cooperate, given that
371 RBPs often bind near splice sites.

372 Finally, our work provides new insights into the relationship between genetic variation, splicing and
373 phenotypic traits. Specifically, we found that sQTLs are enriched in variants associated with a number of
374 complex traits and diseases, some of them previously reported^{9,10,14,15}. sQTLs display stronger GWAS as-
375 sociations than variants not associated with splicing and, for some traits, even larger effects than variants
376 affecting exclusively gene expression. This grants splicing a key role in mediating the impact of genetic
377 variation in human phenotypes¹⁵. Because gene expression is the main driver of biological function, we
378 hypothesize that genetic variants affecting expression are likely to have a much larger biological impact
379 than those affecting splicing: often, they could be lethal during development. In contrast, genetic variants
380 affecting splicing may have subtler effects, therefore being better tolerated and leading more frequently
381 to observable phenotypes. That genetic variants affecting splicing may underlay most human hereditary
382 diseases has already been pointed out¹⁹. Especially relevant seems the implication of sQTLs in the mech-
383 anisms underlying autoimmune diseases, also supported by the overrepresentation of immune functions
384 among sGenes. Actually, sQTLs have been recently proposed as relevant players in human immune re-
385 sponse and its evolution¹⁶. In addition, sQTLs altering RBP binding seem to play a prominent role in
386 disease. Indeed, the relevance of RBPs in human disorders has been often remarked⁶².

387 A more detailed analysis of the relationship between sQTLs and GWAS variants could be achieved by
388 the usage of statistical methods to assess co-localization^{63–65}, and subsequent fine-mapping of the sQTL
389 candidates^{66–68} to assign causal probabilities. However, currently available methods are not directly ap-
390 plicable within our multivariate, non-parametric framework. In addition, recent works have demonstrated
391 the utility of *in silico* splicing predictors to identify pathogenic variants affecting splicing, especially in the
392 case of Mendelian disorders^{69–71}. These methods provide a complementary view to RNA-seq-based ap-
393 proaches that measure splicing changes associated with genetic variants, such as sQTLseeker2. Indeed,
394 while the former target rare variants in the vicinity of splice sites with strong phenotypic effects, the latter
395 focus on common regulatory variation, not restricted to the splice region nor necessarily pathogenic. Fur-
396 thermore, the ability of pathogenicity predictors to account for features such as evolutionary conservation
397 or exon importance provides valuable information about the relevance of individual alleles⁷¹, which may
398 help prioritizing sQTLs in clinical settings.

399 Our implementation of an enhanced pipeline for sQTL mapping based on `sQTLseeker2`, `Nextflow` and
400 Docker will help sQTL discovery in multiple datasets, across different platforms, in a highly parallel and
401 reproducible manner. Here we have employed it to identify sQTLs in the GTEx dataset. The extensive
402 catalogue of sQTLs generated constitutes a highly valuable resource for the field. As our initial analyses
403 already show, this resource will contribute to the understanding of the mechanisms underlying alternative
404 splicing regulation and its implication in phenotypic traits, including disease risk.

Data availability

All the data employed in this study is publicly available. GTEx data was obtained from dbGaP (www.ncbi.nlm.nih.gov/gap/, accessions *phs000424.v7.p2* and *phs000424.v8.p2*). ENCODE and ENTEEx data was obtained from the ENCODE Portal (www.encodeproject.org, accession numbers provided in Supplementary Tables S5-7). The sQTL catalogue generated is available at https://public-docs.crg.es/rguigo/Data/dgarrido/sQTLs.GarridoMartin_etal.tar.gz.

Code availability

Our pipeline for sQTL mapping is publicly available at <https://github.com/dgarrimar/sqtlseeker2-nf>. Detailed information about the software can be found in Methods and Supplementary Note 1.

1 Methods

2 GTEx data

3 Transcript expression (transcripts per million, TPM) and variant calls (SNPs and short *indels*) were obtained
4 from the V7 release of the Genotype-Tissue Expression (GTEx) Project (dbGaP accession *phs000424.v7.p2*).
5 These correspond to 10,361 samples from 620 deceased donors with both RNA-seq in up to 53 tis-
6 sues and Whole Genome Sequencing (WGS) data available. Metadata at donor and sample level and
7 variant annotations (Ensembl's Variant Effect Predictor, VEP, v83 (<http://www.ensembl.org/info/docs/tools/vep>) with the Loss-Of-Function Transcript Effect Estimator extension, LOFTEE, (<https://github.com/konradjk/loftee>)) were also retrieved. In GTEx V7, RNA-seq reads are aligned to
8 the human reference genome (build hg19/GRCh37) using STAR⁷² v2.4.2a, based on the GENCODE v19
9 annotation (https://www.gencodegenes.org/human/release_19.html). Transcript-level quantifi-
10 cations are obtained with RSEM⁷³ v1.2.22. WGS reads are aligned with BWA-MEM ([http://bio-bwa.](http://bio-bwa.sourceforge.net)
11 sourceforge.net) after base quality score recalibration and local realignment at known *indels* us-
12 ing Picard (<http://broadinstitute.github.io/picard>). Joint variant calling across all samples
13 is performed using GATK's HaplotypeCaller v3.4 (<https://software.broadinstitute.org/gatk/documentation/tooldocs>). Further details on GTEx data preprocessing and QC pipelines can be
14 found on the GTEx Portal (<https://gtexportal.org>).
15

16 sQTL mapping

17 Gene, transcript and variant filtering

18 48 tissues with sample size $n \geq 70$ were selected for *cis* sQTL mapping. The *cis* window was defined as the
19 gene body plus 5 Kb upstream and downstream the gene boundaries. We considered genes expressed
20 ≥ 1 TPM in at least 80% of the samples (samples with lower gene expression were removed from the
21 analysis of the gene), with at least two isoforms and a minimum isoform expression of 0.1 TPM (transcripts
22 with lower expression in all samples were removed). These filters correspond to the default parameters of
23 sQTLseekeR2. We analyzed only biallelic SNPs and short *indels* (autosomal + X) with MAF ≥ 0.01 and
24 at least 10 samples per observed genotype group. In total, 3,588,609 variants and 16,010 genes (15,195
25 protein-coding, 815 lincRNA) were analyzed.
26

27 Covariate selection

28 To evaluate the impact of known technical and biological covariates at sample and donor level in expression
29 data, we regressed the first ten principal components (PCs) of the gene expression per tissue onto each
30 available covariate, determining the percentage of variance explained (R^2_{adj}). We selected donor ischemic
31 time, gender and age, as well as sample RIN (RNA integrity number) as the most relevant covariates. We
32 also included the first three genotype PCs (obtained from dbGap and computed as described in [24]), to
33

34 control for population (i.e. ancestry) effects, and the genotyping platform employed (Illumina HiSeq 2000 or
35 HiSeq X). Selected covariates were regressed out from the relative abundances of each gene's transcript
36 isoforms by `sQTLseeker2` before testing for association with the genotype.

37 **Software**

38 For sQTL mapping we employed `sQTLseeker2` v1.0.0, an enhanced version (see also Supplementary
39 Note 1) of the `sQTLseeker` R package²⁰, which identifies genetic variants that are associated with multi-
40 variate changes in the relative abundances of a gene's transcript isoforms (i.e. splicing ratios). `sQTLseeker2`
41 was embedded in `sqt1seeker2-nf`, a highly parallel, portable and reproducible pipeline for sQTL map-
42 ping developed using Nextflow²³, a framework for computational workflows, and Docker container technol-
43 ogy. `sQTLseeker2` and `sqt1seeker2-nf` are available at <https://github.com/dgarrimar>.

44 **Details on significance assessment**

45 We performed *cis* sQTL mapping on each tissue. Nominal *p* values were obtained using the function
46 `sqt1.seeker`. To correct for the fact that multiple genetic variants in LD were tested per gene, an adaptive
47 permutation scheme was applied (implemented in the function `sqt1.seeker.p`). A Benjamini-Hochberg
48 false discovery rate (FDR) threshold of 0.05 was selected to identify sGenes. To retrieve all significant
49 variant-gene pairs, we employed a procedure identical to the one described in [24] for expression QTLs
50 (implemented in the function `sqt1s.p`). See Supplementary Note 1 for details. In addition, as our test
51 statistic is sensitive to the heterogeneity of the splicing ratios' variability among genotype groups, a multi-
52 variate homoscedasticity test⁷⁴ was also performed for each gene-variant pair. Pairs failing this test (FDR
53 across all nominal tests > 0.05) were still assessed for significance and taken into account for multiple
54 testing correction, but they were not reported as significant sQTLs.

55 **Cell type heterogeneity**

56 We employed xCell²⁵ to estimate the enrichment of 64 reference cell types from the bulk expression profile
57 of each GTEx sample. We applied the `xCellAnalysis` function in the `xCell` R package to the full gene
58 expression TPM matrix (56,205 genes \times 11,688 samples), in order to maximize tissue heterogeneity. We
59 then applied the τ index³¹ (see also section *sQTL sharing*) to median xCell enrichments across samples
60 per tissue. The cell type heterogeneity of a tissue was estimated as $1 - \tau$. While these results should be
61 interpreted with caution, as xCell is not a deconvolution method, but an enrichment method, they were
62 generally biologically meaningful. For example, the most homogeneous tissues included brain subregions
63 or transformed fibroblasts, and the most heterogeneous, spleen or whole blood. To determine the impact of
64 the cell type heterogeneity of a tissue on sQTL discovery, we computed the partial correlation between the
65 number of sGenes over the number of tested genes and the estimated cell type heterogeneity (i.e. $1 - \tau$),
66 controlling for the tissue sample size.

67 sQTL effect size

68 We used the absolute maximum difference (MD) in mean adjusted transcript relative expression between
69 genotype groups as a measure of the size of the effect. MD takes values in the interval [0, 1]. In practice,
70 usual MD values belong to [0.01, 0.4]. As a general rule, we considered MD values < 0.1 as *small* effect
71 sizes, MD values between 0.1 and 0.2 as *moderate* effect sizes and MD values greater than 0.2 as *large*
72 effect sizes. sQTLs with MD values below 0.05 were not taken into account for further analyses (default in
73 sQTLseeker2).

74 GO enrichment of sGenes

75 For each tissue, we obtained the corresponding set of sGenes, and performed hypergeometric tests to
76 assess Gene Ontology (GO) Biological Process (BP) term over-representation, selecting as gene universe
77 all the tested genes. We set a FDR threshold of 0.1 to identify significantly enriched terms. Similarly, we
78 selected genes that were not sGenes in any tissue, and performed a hypergeometric test to assess GO BP
79 term over-representation in this set (FDR < 0.1, universe: all tested genes). Then, we employed REVIGO⁷⁵
80 (<http://revigo.irb.hr/>, with parameters: allowed similarity = 0.9, database = *H. sapiens*, semantic
81 metric = *SimRel*) to remove highly redundant terms and generate semantic similarity-based GO term
82 representations for sGenes and non-sGenes.

83 sQTL replication

84 To assess replication of GTEx sQTLs, we examined the *p* values for matched variant-gene pairs identified
85 as splicing QTLs by sQTLseeker for three immune cell types (CD14⁺ monocytes, CD16⁺ neutrophils, and
86 naive CD4⁺ T cells) in the Blueprint Project (BP)²⁷. Both studies have large differences in RNA sources
87 (tissues in GTEx vs cell types in Blueprint), library preparation (unstranded polyA⁺ vs stranded Ribo-Zero),
88 sequencing strategy (e.g. paired-end vs single-end in monocytes and neutrophils) and data processing
89 pipelines (e.g. different transcript quantification software). π_1 statistics, that provide an estimate of the
90 proportion of true positives⁷⁶, were computed for each pair GTEx tissue/BP celltype. A final replication rate
91 for each GTEx tissue was calculated as the average π_1 value across the three BP cell types.

92 Alternative splicing events associated with sQTLs

93 To determine the nature of the splicing events related to sQTLs we selected, for each sQTL, the two
94 isoforms of the target sGene that changed the most (in opposite directions) across genotypes. Then, we
95 compared the exonic structure of both transcripts using the function `classify.events` of sQTLseeker,
96 which extends the classification proposed in AStalavista⁷⁷. We considered the same event categories
97 depicted in Monlong et al.²⁰: exon skipping, alternative 5' and 3' splice sites, intron retention, mutually
98 exclusive exons, alternative first and last exons, alternative 5' and 3' UTR, tandem 5' and 3' UTRs, complex
99 splicing events (complex combinations of events affecting internal exons) and complex 5'/3' events (complex

100 combinations of events affecting 5'/3' termini). Some of these events are not explicitly involving splicing, but
101 alternative transcription initiation and termination sites. Note that each transcript pair, and therefore each
102 sQTL, can be associated with more than one event.

103 **Heteropletropy and ENTEX histone modification analysis**

104 Given a genetic variant v and a pair of genes (i.e. g_1 and g_2) and tissues (i.e. t_1 and t_2), we consider
105 v heteropletropic with effects in different tissues if i) v is an sQTL -but not an eQTL- for gene g_1 in
106 tissue t_1 , ii) v is an eQTL -but not an sQTL- for gene g_2 in tissue t_2 , iii) v is neither an sQTL nor an
107 eQTL for gene g_2 in tissue t_1 and iv) v is neither an sQTL nor an eQTL for gene g_1 in tissue t_2 . Out
108 of 148,618 variants tested for association with both the expression and splicing of at least two genes in
109 at least two tissues, we identified 6,552 heteropletropic cases. In order to evaluate whether changes
110 at epigenetic level were occurring at these positions, we obtained ChIP-seq peaks corresponding to six
111 histone modifications (H3K27ac, H3K4me1, H3K4me3, H3K36me3, H3K27me3 and H3K9me3) from the
112 ENTEX data collection of the ENCODE Project^{78,79} (<https://www.encodeproject.org/>, accessed
113 2019-10-04, accession numbers provided in Table S5). ENTEX is a joint effort between GTEx and ENCODE
114 consortia to deeply profile overlapping tissues from the same four donors (two male, two female) using
115 shared technologies. The two tissues of interest were available for at least 3 out of 4 ENTEX donors
116 for 2,855 heteropletropic variants. By overlapping these with the ChIP-seq peaks in the corresponding
117 tissues, we identified 699 cases where one or more histone marks present in a tissue were absent in the
118 other (in at least 3 donors). We compared this number with the one obtained for variants v' affecting both
119 the splicing and expression of the two genes (g_1 and g_2) in the two tissues (t_1 and t_2), using Fisher's exact
120 test for significance assessment.

121 **sQTL sharing**

122 For every pair of tissues, we selected variant-gene pairs tested in both and found significant in at least
123 one. We computed *Pearson* correlation (r) between their effect sizes (MD values). Tissue specificity was
124 estimated as $s_t = 1 - \bar{r}_t$, where \bar{r}_t is the mean correlation between a given tissue t and the others. To
125 determine the robustness of the observed sharing patterns with changes in the sample size, we randomly
126 downsampled every original tissue dataset once to 100, 200 and 300 samples, ran our sQTL mapping
127 pipeline again and re-evaluated the sharing patterns. Alternatively, we computed the *Jaccard* index on
128 the sets of variant-gene pairs identified in every pair of tissues. In this case, tissue specificity estimates
129 corresponded to $1 - \bar{j}_t$, where \bar{j}_t is the mean *Jaccard* index between a given tissue t and the others.

130 We further compared these approaches with a third strategy, aimed at evaluating the changes in the
131 whole splicing phenotype due to sQTLs between different tissues, rather than relying on MD values or sQTL
132 presence/absence. This allows more flexibility, likely resulting in an increased ability to capture complex
133 sharing patterns. In short, we focused on variant-gene pairs tested in all tissues and found significant in
134 at least one. For every tissue t_i , variant-gene pair $j \in \{1 \dots p\}$, and genotype group $k \in \{0, 1, 2\}$, we

135 computed the centroid of the adjusted (square root transformed, covariate corrected) splicing ratios, $c_{t,ijk}$.

136 Then, we obtained:

$$d(t_1, t_2) = \frac{1}{p} \sum_{j=1}^p \sum_{k=0}^2 \|c_{t_1jk} - c_{t_2jk}\|$$

137 where d measures the distance between any two tissues (t_1 and t_2) in terms of sQTL sharing, as the
138 mean (across variant-gene pairs) of the sum (across genotype groups) of the Euclidean distance between
139 centroids ($\|x\|$ represents the Euclidean norm of vector x). Small values of d correspond to large sQTL
140 sharing, and vice versa (Fig. S9a illustrates the behaviour of d for a single variant-gene pair evaluated in 4
141 tissues). A distance matrix built upon d values was then employed as input for hierarchical clustering.

142 To compare the tissue clusters obtained using different approaches we computed Baker's Gamma
143 (Γ), a metric of similarity between two dendograms given by the rank correlation between the stages at
144 which pairs of objects combine in each of the two trees⁸⁰. Γ ranges from -1 to 1, with values close to 1
145 corresponding to high similarity between both dendograms. To assess the significance of this similarity,
146 we performed a permutation test (shuffling the labels of one tree 10,000 times, keeping tree topologies
147 constant). We also employed Baker's Gamma to compare our trees with the one obtained using `mashR`³⁰ for
148 LeafCutter sQTLs in GTEx V8¹², available at <https://github.com/broadinstitute/gtex-v8>.

149 Of note, we employed pairwise approaches to study sQTL sharing, rather than methods to analyze QTL
150 sharing jointly across tissues (such as `mashR`, to cite an example), given that the latter, to the best of our
151 knowledge, cannot be applied in our multivariate, non-parametric setting.

152 In addition, for each sGene tested in all tissues and found significant in at least one, we determined
153 tissue specificity of the sGene expression, using the τ index³¹:

$$\tau = \frac{\sum_{t=1}^n (1 - \hat{x}_t)}{n - 1}; \quad \hat{x}_t = \frac{x_t}{\max_{1 \leq t \leq n} (x_t)}$$

154 where x_t is the expression of the gene in tissue t and n the number of tissues. τ takes values between
155 0 (i.e. genes equally expressed in all tissues) and 1 (i.e. tissue-specific genes). We calculated τ using
156 median gene expression across tissues. In addition, to assess tissue specificity of splicing regulation, we
157 computed a variation of τ , τ_s , where x_t was the $-\log_{10}(\text{FDR})$ of the sGene in tissue t . For sGenes in the
158 top 20 percentile of the distribution of τ_s values, and the bottom 20 percentile of the distribution of τ values,
159 we evaluated GO BP term over-representation (hypergeometric test, FDR < 0.1, universe: all sGenes).

160 Functional enrichment of sQTLs

161 ChIP-seq peaks (transcription factor binding sites, histone marks) and open-chromatin regions were ob-
162 tained from the Ensembl Regulation dataset (<ftp://ftp.ensembl.org/pub/grch37/release-86/>
163 regulation/homo_sapiens). eCLIP peaks in HepG2 and/or K562 cell lines for 114 RNA-binding pro-
164 teins (RBPs)³⁴ were obtained from the ENCODE Project^{78,79} (<https://www.encodeproject.org>, see

165 section *Splice site strength and sQTL impact on RBP binding sites* for details). Disease and complex-trait
166 associated variants were retrieved from the GWAS catalog (<https://www.ebi.ac.uk/gwas>, accessed
167 2018-09-18), extended to GTEx variants in high linkage disequilibrium ($r^2 > 0.8$) with the GWAS hits.
168 Protein coding and lincRNA exons were derived from the GENCODE v19 annotation. The coordinates of
169 these functional elements were overlapped with all the tested variants (either sQTLs or not) to obtain a
170 functional annotation per variant. The functional consequences of each variant (stop-gained, frameshift,
171 etc.), computed by the Variant Effect Predictor (VEP, <http://www.ensembl.org/info/docs/tools/vep>),
172 were obtained from dbGap (accession *phs000424.v7.p2*). Note that the VEP leverages the En-
173 sembl Variation dataset, which contains data from a wide variety of sources (https://www.ensembl.org/info/genome/variation/species/sources_documentation.html). From the VEP result
174 we also identified variants with *HIGH* impact or in the categories *probably damaging* (PolyPhen, <http://genetics.bwh.harvard.edu/pph2>), *deleterious* (SIFT, <https://sift.bii.a-star.edu.sg>),
175 *pathogenic* (ClinVar, <https://www.ncbi.nlm.nih.gov/clinvar>) and *high-confidence loss-of-function*
176 (LOFTEE, <https://github.com/konradjk/loftee>).

177 The top 10 most significant sQTLs per gene and tissue were compared to a null distribution of 1000
178 sets of randomly sampled variants not associated with splicing (FDR > 0.05, *non-sQTLs*), with the same
179 size of the sQTL set. The top 10 were selected to ensure the coverage of the less common annotations.
180 Non-sQTLs were matched to sQTLs in terms of relative location within the gene and minor allele frequency
181 (MAF). Specifically, we selected non-sQTLs so that they were located in the same bins (see section *sQTL*
182 *location*) within the genes for which they were not sQTLs, as sQTLs within the genes for which they were
183 sQTLs, and had MAFs equal to the sQTLs' MAFs +/- 0.02. The enrichment was calculated as the odds
184 ratio (OR) of the frequency of a certain annotation among sQTLs to the mean frequency of the same
185 annotation across the 1000 non-sQTLs sets. To ensure enrichment reliability, we filtered out annotations
186 with a mean frequency across the non-sQTLs sets lower than 5. The significance of each enrichment
187 was assessed using a Fisher's exact test. *p* values were corrected for false discovery rate, selecting a
188 threshold of FDR < 0.05. Enrichments in a subset of relevant features, such as high impact/potentially
189 damaging variants, splice sites, GWAS hits, exons, TFBS (all TFs pooled together), RBP binding sites (all
190 RBPs pooled together), Pol II binding sites, HK36me3 and open chromatin regions, were also carried out
191 separately for high effect size (MD ≥ 0.2) and low effect size sQTLs (MD < 0.1).

194 sQTL location

195 We divided every sGene body into 20 bins of equal size and assigned each sQTL to the corresponding bin
196 according to its location. The number of bins (20) was selected in order to provide a good balance between
197 granularity and bin size. We computed the mean proportion of sQTLs (with respect to the total number of
198 sQTLs for the gene) on each bin. An identical procedure was applied to exons, introns, downstream and
199 upstream regions. In each case, to ensure a minimum bin size, we filtered out the 20% shortest regions.
200 Under the null hypothesis of no preference in location, a uniform distribution for the mean proportion of

201 sQTLs across bins was expected.

202 **Splice site strength and sQTL impact on RBP binding sites**

203 To estimate the impact of genetic variants on splice sites, for each variant (either sQTL or not) within the
204 sequence of an annotated splice site we scored the site considering the reference and the alternative al-
205 lele, using position weight matrices (PWMs) built upon human splice sites⁸¹. High scores corresponded to
206 common/strong splice sites, while low scores corresponded to rare/weak sites, probably leading to less ef-
207 ficient splicing. Then we estimated the change in splice site strength as the absolute value of the difference
208 between alternative and reference scores.

209 To estimate the impact of genetic variants on RBP binding sites, we obtained eCLIP peaks in HepG2 and
210 K562 cell lines for 114 RBPs³⁴ from the ENCODE Project^{78,79} (<https://www.encodeproject.org/>,
211 accessed 2018-04-16, accession numbers provided in Table S6). For each RBP, we selected the peaks
212 significant at $FDR < 0.01$ and with a fold-change (FC) with respect to the mock input ≥ 2 . We further
213 required a minimum overlap between replicates (50% of the length of the union of a given pair of peaks).
214 This constituted our positive set of RBP-binding sequences. We generated an equally-sized negative set
215 of matched (in terms of GC content, length and repeats) sequences, not overlapping eCLIP peaks from
216 the same RBP. We combined both sets of sequences to build our training set. To achieve feasible memory
217 usage and running times, we limited the size of the training set to 30,000 sequences.

218 We then trained a gapped k-mer support vector machine (gkm-SVM)³⁷ with default parameters (word
219 length $l = 10$, informative columns $k = 6$), as recommended for our training set size range³⁶. Other
220 choices of l and k barely changed the overall performance (Fig. S23). The option `addRC` (add reverse
221 complementary) was set to FALSE as we were working with RNA sequences. The classification perfor-
222 mance was evaluated using a 5-fold cross-validation. 79 RBPs with a mean cross-validation area under
223 the Receiver Operating Characteristic curve (ROC AUC) ≥ 0.8 were kept. To predict the impact of variants
224 in RBP binding, for all the variants overlapping the eCLIP peaks ($FDR < 0.01$, $FC \geq 2$) of a given RBP, we
225 computed the deltaSVM metric³⁶. The gkmSVM assigns a weight to each possible 10-mer, quantifying its
226 contribution to the prediction of RBP binding. Each variant is given a score computed as the sum of the
227 weights of the 10-mers overlapping it (10-mer SVM scores were used as a proxy for weights). deltaSVM
228 computes the difference between the score of the alternative and the reference allele, quantifying their
229 difference in predictive potential. Here we used the minor and the major allele instead of the alternative
230 and the reference allele, respectively.

231 We focused on the most predictive variants of the binding of each RBP (score of the variant at ei-
232 ther allele among the 5% highest scores for this RBP). This was done to target those variants lying
233 on sequences likely to be highly relevant for RBP binding (i.e. potential binding sites). To ensure the
234 robustness of our results, we further required at least 30 sQTLs with deltaSVM values per RBP, re-
235 sulting in a final set of 32 RBPs. Of these, for 12 RBPs with significantly different $|\text{deltaSVM}|$ values
236 between sQTLs and non-sQTLs (Wilcoxon Rank-Sum test, $FDR < 0.1$), we obtained the 100 highest-

237 scoring 10-mers, aligned them using mafft v7.407 (high accuracy mode *L-INS-1*)⁸², removed the columns
238 of the alignment with more than 50% of gaps and built sequence logos using WebLogo standalone v3.6.0
239 (<http://weblogo.threeplusone.com/>).

240 To evaluate allele-specific RBP binding (ASB), we obtained the ASB variants identified in the same
241 eCLIP dataset using BEAPR (Binding Estimation of Allele-specific Protein-RNA interaction), available from
242 Yang et al.³⁸. In short, BEAPR is a method to identify ASB events in protein-RNA interactions from eCLIP
243 data. It accounts for crosslinking-induced sequence propensity and variability between replicates, outper-
244 forming commonly used count-based approaches. We only considered ASB variants for which the same
245 alleles had been genotyped in GTEx. We focused on sQTLs, non-sQTLs and ASB variants overlapping
246 eCLIP peaks (FDR < 0.01, FC \geq 2) for any of the 114 RBPs of interest in HepG2 and/or K562 cell lines.
247 We assessed the significance of the difference in the proportion of sQTLs and non-sQTLs overlapping ASB
248 variants across RBPs using Fisher's exact test. We also performed this analysis separately for each RBP,
249 using false discovery rate for multiple testing correction (FDR < 0.05).

250 co- and post- transcriptional splicing

251 We obtained RNA-seq data from nuclear and cytoplasmic fractions (2 replicates/fraction) corresponding
252 to 13 cell lines available from the ENCODE project^{78,79} (<https://www.encodeproject.org/>, ac-
253 cessed 2018-05-25, accession numbers provided in Table S7). A nextflow implementation of the Inte-
254 grative Pipeline for Splicing Analyses (IPSA), developed *in house* ([https://github.com/guigolab/](https://github.com/guigolab/ipsa-nf)
255 *ipsa-nf*), was employed to determine the number of reads supporting splicing completion and splicing
256 incompleteness, for each intron annotated in GENCODE v19. We excluded from this analysis introns that
257 overlapped either exons or non-identical introns in terms of chromosome, start and end positions. To as-
258 sess the significance of the difference in the proportion of reads supporting splicing completion between
259 nuclear and cytoplasmic compartments we employed Fisher's exact test. False discovery rate was em-
260 ployed for multiple testing correction (FDR < 0.05). Introns with significantly larger proportions of reads
261 supporting splicing completion in the cytoplasm were classified as post-transcriptionally spliced (here re-
262 ferred to as *ps*). Introns that did not pass the FDR threshold were labelled as either unprocessed (i.e. intron
263 retention events) or co-transcriptionally spliced (here referred to as *cs*), depending on the degree of splicing
264 completion in both cellular compartments. We focused on introns consistently classified as either *ps* or *cs*
265 in at least 10 of the analyzed cell lines. We computed variant density (number of variants per Kb of intron)
266 at 10 bins of equal size along both types of introns (10 was selected to ensure that enough variants were
267 present in each bin). We also assessed the enrichment in functional elements of sQTLs in *ps* introns with
268 respect to sQTLs in *cs* using Fisher's exact test. False discovery rate was employed for multiple testing
269 correction (FDR < 0.05).

270 GWAS analyses

271 We downloaded the GWAS catalog, including the Experimental Factor Ontology (EFO) annotations for
272 the GWAS terms (<https://www.ebi.ac.uk/gwas>, accessed 2018-09-18). We used LiftOver (<https://genome.ucsc.edu/cgi-bin/hgLiftOver>) to convert variant coordinates from hg38 to hg19 and
273 PLINK v1.90b6.2 (<https://www.cog-genomics.org/plink2>) to extend the catalog to the variants in
274 high linkage disequilibrium ($r^2 \geq 0.8$) with the GWAS hits. The sQTL enrichment was calculated as the
275 odds ratio (OR) of the frequency of GWAS variants among sQTLs to the mean frequency of GWAS vari-
276 ants across 1000 matched non-sQTL sets (see section *Functional enrichment of sQTLs*). In parallel, we
277 obtained the complete EFO ontology (<https://www.ebi.ac.uk/efo/>) in Open Biomedical Ontologies
278 (OBO) format. For the GWAS terms with an OR > 1, we used the `ontologySimilarity` R package⁸³ to
279 compute the pairwise semantic similarity (method = `resnik`) between the enriched GWAS terms, and built
280 a similarity matrix, S . From it, we derived a distance matrix, D , as $\max(S) - S$, and performed multi-
281 dimensional scaling (MDS). This is an analogous strategy to the one employed in REVIGO⁷⁵ to visualize GO
282 terms.

284 We further compiled genome-wide GWAS summary statistics for 8 traits representative of the clus-
285 ters observed in the MDS representation: asthma⁴², breast cancer⁴³, coronary artery disease⁴⁴, heart
286 rate⁴⁵, height⁴⁶, LDL cholesterol levels⁴⁷, rheumatoid arthritis⁴⁸ and schizophrenia⁴⁹. In each case, we
287 employed `fgwas`⁵⁰ v0.3.6 (<https://github.com/joepickrell/fgwas>, default parameters, except
288 for window size set to 2500bp to ensure convergence) to obtain the maximum likelihood estimate and
289 95% confidence interval for the association effect size, both for i) sQTLs (variants affecting splicing, inde-
290 pendently of their effect on expression), and ii) variants affecting expression, but not splicing (GTEx V7
291 eQTLs tested also in our setting and not identified as sQTLs). To display the regional GWAS associa-
292 tion results for the GSDMB locus we employed LocusZoom standalone v1.4 (<https://github.com/>
293 `statgen/locuszoom-standalone`).

References

1. Nilsen, T. W. & Graveley, B. R. Expansion of the eukaryotic proteome by alternative splicing. *Nature* **463**, 457–463 (2010).
2. Keren, H., Lev-Maor, G. & Ast, G. Alternative splicing and evolution: diversification, exon definition and function. *Nature Reviews Genetics* **11**, 345–55 (2010).
3. Scotti, M. M. & Swanson, M. S. RNA mis-splicing in disease. *Nature Reviews Genetics* **17**, 19–32 (2016).
4. Chen, M. & Manley, J. L. Mechanisms of alternative splicing regulation: insights from molecular and genomics approaches. *Nature Reviews Molecular cell biology* **10**, 741–754 (2009).
5. Fu, X.-D. & Ares, M. Context-dependent control of alternative splicing by RNA-binding proteins. *Nature Reviews Genetics* **15**, 689–701 (2014).
6. Kornblihtt, A. R. *et al.* Alternative splicing: a pivotal step between eukaryotic transcription and translation. *Nature Reviews Molecular Cell Biology* **14**, 153–165 (2013).
7. Lappalainen, T. *et al.* Transcriptome and genome sequencing uncovers functional variation in humans. *Nature* **501**, 506–11 (2013).
8. Battle, A. *et al.* Characterizing the genetic basis of transcriptome diversity through RNA-sequencing of 922 individuals. *Genome Research* **24**, 14–24 (2014).
9. Takata, A., Matsumoto, N. & Kato, T. Genome-wide identification of splicing QTLs in the human brain and their enrichment among schizophrenia-associated loci. *Nature Communications* **8**, 14519 (2017).
10. Raj, T. *et al.* Integrative transcriptome analyses of the aging brain implicate altered splicing in Alzheimer's disease susceptibility. *Nature Genetics* **50**, 1584–1592 (2018).
11. Tian, J. *et al.* CancerSplicingQTL: a database for genome-wide identification of splicing QTLs in human cancer. *Nucleic Acids Research* **47**, D909–D916 (2019).
12. The GTEx Consortium. The GTEx Consortium atlas of genetic regulatory effects across human tissues. *bioRxiv*, 787903 (2019).
13. Ma, L., Jia, P. & Zhao, Z. Splicing QTL of human adipose-related traits. *Scientific reports* **8**, 318 (2018).
14. Caswell, J. L. *et al.* Multiple breast cancer risk variants are associated with differential transcript isoform expression in tumors. *Human Molecular Genetics* **24**, 7421–31 (2015).
15. Li, Y. I. *et al.* RNA splicing is a primary link between genetic variation and disease. *Science* **352**, 600–604 (2016).
16. Rotival, M., Quach, H. & Quintana-Murci, L. Defining the genetic and evolutionary architecture of alternative splicing in response to infection. *Nature Communications* **10**, 1671 (2019).
17. Ongen, H. & Dermitzakis, E. T. Alternative Splicing QTLs in European and African Populations. *American Journal of Human Genetics* **97**, 567–75 (2015).

18. Li, Y. I. *et al.* Annotation-free quantification of RNA splicing using LeafCutter. *Nature Genetics* **50**, 151–158 (2018).
19. López-Bigas, N., Audit, B., Ouzounis, C., Parra, G. & Guigó, R. Are splicing mutations the most frequent cause of hereditary disease? *FEBS Letters* **579**, 1900–1903 (2005).
20. Monlong, J., Calvo, M., Ferreira, P. G. & Guigó, R. Identification of genetic variants associated with alternative splicing using sQTLseekeR. *Nature Communications* **5**, 4698 (2014).
21. Anderson, M. A new method for non-parametric multivariate analysis of variance. *Australian Ecology* **26**, 32–46 (2001).
22. Anderson, M. J. & Robinson, J. Generalized discriminant analysis based on distances. *Australian & New Zealand Journal of Statistics* **45**, 301–318 (2003).
23. Di Tommaso, P. *et al.* Nextflow enables reproducible computational workflows. *Nature Biotechnology* **35**, 316–319 (2017).
24. The GTEx Consortium. Genetic effects on gene expression across human tissues. *Nature* **550**, 204–213 (2017).
25. Aran, D., Hu, Z. & Butte, A. J. xCell: Digitally portraying the tissue cellular heterogeneity landscape. *Genome Biology* **18**, 220 (2017).
26. Jangi, M. & Sharp, P. Building Robust Transcriptomes with Master Splicing Factors. *Cell* **159**, 487–498 (2014).
27. Chen, L. *et al.* Genetic Drivers of Epigenetic and Transcriptional Variation in Human Immune Cells. *Cell* **167**, 1398–1414 (2016).
28. Reyes, A. & Huber, W. Alternative start and termination sites of transcription drive most transcript isoform differences across human tissues. *Nucleic Acids Research* **46**, 582–592 (2018).
29. The GTEx Consortium. The Genotype-Tissue Expression (GTEx) pilot analysis: multitissue gene regulation in humans. *Science* **348**, 648–60 (2015).
30. Urbut, S. M., Wang, G., Carbonetto, P. & Stephens, M. Flexible statistical methods for estimating and testing effects in genomic studies with multiple conditions. *Nature Genetics* **51**, 187–195 (2019).
31. Yanai, I. *et al.* Genome-wide midrange transcription profiles reveal expression level relationships in human tissue specification. *Bioinformatics* **21**, 650–659 (2005).
32. Adzhubei, I. A. *et al.* A method and server for predicting damaging missense mutations. *Nature Methods* **7**, 248–249 (2010).
33. Sim, N.-L. *et al.* SIFT web server: predicting effects of amino acid substitutions on proteins. *Nucleic Acids Research* **40**, W452–W457 (2012).
34. Van Nostrand, E. L. *et al.* Robust transcriptome-wide discovery of RNA-binding protein binding sites with enhanced CLIP (eCLIP). *Nature Methods* **13**, 508–514 (2016).

35. Ghandi, M., Lee, D., Mohammad-Noori, M. & Beer, M. A. Enhanced Regulatory Sequence Prediction Using Gapped k-mer Features. *PLOS Computational Biology* **10** (2014).
36. Lee, D. *et al.* A method to predict the impact of regulatory variants from DNA sequence. *Nature Genetics* **47**, 955–961 (2015).
37. Ghandi, M. *et al.* gkmSVM: an R package for gapped-kmer SVM. *Bioinformatics* **32**, 2205–7 (2016).
38. Yang, E.-W. *et al.* Allele-specific binding of RNA-binding proteins reveals functional genetic variants in the RNA. *Nature Communications* **10**, 1338 (2019).
39. Wickramasinghe, V. O. *et al.* Regulation of constitutive and alternative mRNA splicing across the human transcriptome by PRPF8 is determined by 5' splice site strength. *Genome Biology* **16**, 201 (2015).
40. Tilgner, H. *et al.* Deep sequencing of subcellular RNA fractions shows splicing to be predominantly co-transcriptional in the human genome but inefficient for lncRNAs. *Genome Research* **22**, 1616–1625 (2012).
41. Malone, J. *et al.* Modeling sample variables with an Experimental Factor Ontology. *Bioinformatics* **26**, 1112–1118 (2010).
42. Demenais, F. *et al.* Multiancestry association study identifies new asthma risk loci that colocalize with immune-cell enhancer marks. *Nature Genetics* **50**, 42–53 (2018).
43. Michailidou, K. *et al.* Association analysis identifies 65 new breast cancer risk loci. *Nature* **551**, 92–94 (2017).
44. Schunkert, H. *et al.* Large-scale association analysis identifies 13 new susceptibility loci for coronary artery disease. *Nature Genetics* **43**, 333–338 (2011).
45. Den Hoed, M. *et al.* Identification of heart rate–associated loci and their effects on cardiac conduction and rhythm disorders. *Nature Genetics* **45**, 621–631 (2013).
46. Wood, A. R. *et al.* Defining the role of common variation in the genomic and biological architecture of adult human height. *Nature Genetics* **46**, 1173–1186 (2014).
47. The Global Lipids Genetics Consortium. Discovery and refinement of loci associated with lipid levels. *Nature Genetics* **45**, 1274–1283 (2013).
48. Okada, Y. *et al.* Genetics of rheumatoid arthritis contributes to biology and drug discovery. *Nature* **506**, 376–81 (2014).
49. Schizophrenia Working Group of the Psychiatric Genomics Consortium. Biological insights from 108 schizophrenia-associated genetic loci. *Nature* **511**, 421–7 (2014).
50. Pickrell, J. Joint Analysis of Functional Genomic Data and Genome-wide Association Studies of 18 Human Traits. *The American Journal of Human Genetics* **94**, 559–573 (2014).

51. Saleh, N. M. *et al.* Genetic association analyses of atopic illness and proinflammatory cytokine genes with type 1 diabetes. *Diabetes/Metabolism Research and Reviews* **27**, 838–43 (2011).
52. McGovern, D. P. B. *et al.* Genome-wide association identifies multiple ulcerative colitis susceptibility loci. *Nature genetics* **42**, 332–7 (2010).
53. Eyre, S. *et al.* High-density genetic mapping identifies new susceptibility loci for rheumatoid arthritis. *Nature genetics* **44**, 1336–40 (2012).
54. Panganiban, R. A. *et al.* A functional splice variant associated with decreased asthma risk abolishes the ability of gasdermin B to induce epithelial cell pyroptosis. *Journal of Allergy and Clinical Immunology* **142**, 1469–1478 (2018).
55. Das, S. *et al.* GSDMB induces an asthma phenotype characterized by increased airway responsiveness and remodeling without lung inflammation. *Proceedings of the National Academy of Sciences of the United States of America* **113**, 13132–13137 (2016).
56. Ding, J. *et al.* Pore-forming activity and structural autoinhibition of the gasdermin family. *Nature* **535**, 111–116 (2016).
57. González-Porta, M., Calvo, M., Sammeth, M. & Guigó, R. Estimation of alternative splicing variability in human populations. *Genome Research* **22**, 528–38 (2012).
58. Melé, M. *et al.* Human genomics. The human transcriptome across tissues and individuals. *Science* **348**, 660–5 (2015).
59. Sibley, C. R. Regulation of gene expression through production of unstable mRNA isoforms. *Biochemical Society Transactions* **42**, 1196–1205 (2014).
60. Bhatt, D. M. *et al.* Transcript dynamics of proinflammatory genes revealed by sequence analysis of subcellular RNA fractions. *Cell* **150**, 279–290 (2012).
61. Pandya-Jones, A. *et al.* Splicing kinetics and transcript release from the chromatin compartment limit the rate of Lipid A-induced gene expression. *RNA* **19**, 811–827 (2013).
62. Gerstberger, S., Hafner, M. & Tuschl, T. A census of human RNA-binding proteins. *Nature Reviews Genetics* **15**, 829–845 (2014).
63. Giambartolomei, C. *et al.* Bayesian Test for Colocalisation between Pairs of Genetic Association Studies Using Summary Statistics. *PLOS Genetics* **10**, e1004383 (2014).
64. Pickrell, J. K. *et al.* Detection and interpretation of shared genetic influences on 42 human traits. *Nature genetics* **48**, 709–17 (2016).
65. Hormozdiari, F. *et al.* Colocalization of GWAS and eQTL Signals Detects Target Genes. *American Journal of Human Genetics* **99**, 1245–1260 (2016).
66. Hormozdiari, F., Kostem, E., Kang, E. Y., Pasaniuc, B. & Eskin, E. Identifying causal variants at loci with multiple signals of association. *Genetics* **198**, 497–508 (2014).

67. Brown, A. A. *et al.* Predicting causal variants affecting expression by using whole-genome sequencing and RNA-seq from multiple human tissues. *Nature Genetics* **49**, 1747–1751 (2017).
68. Wen, X., Lee, Y., Luca, F. & Pique-Regi, R. Efficient Integrative Multi-SNP Association Analysis via Deterministic Approximation of Posteriors. *American Journal of Human Genetics* **98**, 1114–1129 (2016).
69. Jaganathan, K. *et al.* Predicting Splicing from Primary Sequence with Deep Learning. *Cell* **176**, 535–548 (2019).
70. Cheng, J. *et al.* MMSplice: modular modeling improves the predictions of genetic variant effects on splicing. *Genome Biology* **20**, 48 (2019).
71. Jagadeesh, K. A. *et al.* S-CAP extends pathogenicity prediction to genetic variants that affect RNA splicing. *Nature Genetics* **51**, 755–763 (2019).
72. Dobin, A. *et al.* STAR: ultrafast universal RNA-seq aligner. *Bioinformatics* **29**, 15–21 (2013).
73. Li, B. & Dewey, C. N. RSEM: accurate transcript quantification from RNA-Seq data with or without a reference genome. *BMC Bioinformatics* **12**, 323 (2011).
74. Anderson, M. J. Distance-based tests for homogeneity of multivariate dispersions. *Biometrics* **62**, 245–253 (2006).
75. Supek, F., Bošnjak, M., Škunca, N. & Šmuc, T. REVIGO Summarizes and Visualizes Long Lists of Gene Ontology Terms. *PLOS ONE* **6**, e21800 (2011).
76. Storey, J. D. & Tibshirani, R. Statistical significance for genomewide studies. *Proceedings of the National Academy of Sciences of the United States of America* **100**, 9440–5 (2003).
77. Sammeth, M., Foissac, S. & Guigó, R. A General Definition and Nomenclature for Alternative Splicing Events. *PLOS Computational Biology* **4**, e1000147 (2008).
78. The ENCODE Project Consortium. An integrated encyclopedia of DNA elements in the human genome. *Nature* **489**, 57–74 (2012).
79. Davis, C. A. *et al.* The Encyclopedia of DNA elements (ENCODE): data portal update. *Nucleic Acids Research* **46**, D794–D801 (2018).
80. Galili, T. dendextend: an R package for visualizing, adjusting and comparing trees of hierarchical clustering. *Bioinformatics* **31**, 3718–3720 (2015).
81. Parra, G., Blanco, E. & Guigó, R. Geneld in Drosophila. *Genome Research* **10**, 511–515 (2000).
82. Katoh, K. & Standley, D. M. MAFFT multiple sequence alignment software version 7: improvements in performance and usability. *Molecular Biology Molecular Biology & Evolution Evolution* **30**, 772–80 (2013).
83. Greene, D., Richardson, S. & Turro, E. ontologyX: a suite of R packages for working with ontological data. *Bioinformatics* **33**, 1104–1106 (2017).

84. Garrido-Martín, D., Palumbo, E., Guigó, R. & Breschi, A. ggsashimi: Sashimi plot revised for browser- and annotation-independent splicing visualization. *PLOS Computational Biology* **14**, e1006360 (2018).
85. Hull, J. *et al.* Identification of Common Genetic Variation That Modulates Alternative Splicing. *PLOS Genetics* **3**, e99 (2007).

Acknowledgements

We thank the donors and their families for their generous gifts of organ donation for transplantation and tissue donations for the GTEx research study. We thank Manuel Muñoz, Emilio Palumbo, Aliaksei Holik, François Aguet and Kristin Ardlie for useful discussions. We thank Romina Garrido for administrative support. This project was supported by the National Human Genome Research Institute of the National Institutes of Health under grants R01MH101814 and 5U24HG009446, as well as by the BIO2015-70777-P grant from the Spanish Ministry of Economy, Industry and Competitiveness (MEIC). The Genotype-Tissue Expression (GTEx) project was supported by the Common Fund of the Office of the Director of the National Institutes of Health (<http://commonfund.nih.gov/GTEx>). D.G-M. is supported by a 'la Caixa'-Severo Ochoa pre-doctoral fellowship (LCF/BQ/SO15/52260001). B.B. is supported by the fellowship 2017FI_B_00722 from the Secretaria d'Universitats i Recerca del Departament d'Empresa i Coneixement (Generalitat de Catalunya) and the European Social Fund (ESF). We thank the ENCODE Consortium and, in particular, Thomas Gingeras', Gene Yeo's and Bradley Bernstein's laboratories for data production. We also acknowledge support of the Spanish Ministry of Economy, Industry and Competitiveness (MEIC) to the EMBL partnership, 'Centro de Excelencia Severo Ochoa', the CERCA Programme / Generalitat de Catalunya and the European Regional Development Fund (ERDF).

Author Information

Contributions

D.G-M. and R.G. conceived and designed the study. D.G-M. implemented the software and analyzed the data. B.B. contributed to several analyses, provided analysis tools and helped with the interpretation of the results. M.C. and F.R. contributed ideas and statistical advice, helping with the design of the software. D.G-M. and R.G. wrote the original draft. All the authors reviewed the final manuscript.

Competing Interests

The authors declare no competing interests.